THE SILICON ISOTOPE COMPOSITION OF THE UPPER CONTINENTAL CRUST

Paul S. Savage[1#]*, R. Bastian Georg[2], Helen M. Williams[3] & Alex N. Halliday[1]

[1]Department of Earth Sciences, University of Oxford, South Parks Road, Oxford, OX1 3AN, UK

[#]now at: Department of Earth and Planetary Sciences, Washington University in St. Louis, One Brookings Drive, St. Louis, MO, USA. Tel: +1-(314)-935-5619 / Fax: +1-(314)-935-7361

[2]Water Quality Centre, Trent University, 1600 West Bank Drive, Peterborough, Ontario, K9J 7B8, Canada

[3]Department of Earth Sciences, Durham University, Science Labs, Durham DH1 3LE, UK

*corresponding author: savage@levee.wustl.edu

ABSTRACT

The upper continental crust (UCC) is the major source of silicon (Si) to the oceans and yet its isotopic composition is not well constrained. In an effort to investigate the degree of heterogeneity and provide a robust estimate for the average Si isotopic composition of the UCC, a representative selection of well-characterised, continentally-derived clastic sediments have been analysed using high-precision MC-ICPMS.

Analyses of loess samples define a narrow range of Si isotopic compositions ($\delta^{30}Si$ = -0.28 to -0.15 ‰). This is thought to reflect the primary igneous mineralogy and predominance of mechanical weathering in the formation of such samples. The average loess $\delta^{30}Si$ is -0.22 ± 0.07 ‰ (2 s.d.), identical to average granite and felsic igneous compositions. Therefore, minor chemical weathering does not resolvably affect bulk rock $\delta^{30}Si$, and loess is a good proxy for the Si isotopic composition of unweathered, crystalline, continental crust.

The Si isotopic compositions of shales display much more variability ($\delta^{30}Si$ = -0.82 to 0.00 ‰). Shale Si isotope compositions do not correlate well with canonical proxies for chemical weathering, such as CIA values, but do correlate negatively with insoluble element concentrations and Al/Si ratios. This implies that more intensive or prolonged chemical weathering of a sedimentary source, with attendant desilicification, is required before resolvable negative Si isotopic fractionation occurs. Shale $\delta^{30}Si$ values that are more positive than those of felsic igneous rocks most likely indicate the presence of marine-derived silica in such samples.

Using the data gathered in this study, combined with already published granite Si isotope analyses, a weighted average composition of $\delta^{30}Si$ = -0.25 ± 0.16 ‰ (2 s.d.) for the UCC has been calculated.

Keywords: Silicon isotopes; upper continental crust; shale; loess; MC-ICPMS

1. INTRODUCTION

Silicon (Si) is the second most common element in the Earth's crust (Wedepohl, 1995; Rudnick and Gao, 2003), and the upper continental crust (UCC) is the major source of primary silica to the oceans; around 85% of marine silica is derived from the continents (Tréguer et al., 1995). The (supracrustal) Si cycle is also intrinsically linked with the carbon cycle because it is a major nutrient for planktonic diatoms which represent ~40% of marine primary productivity (e.g. Tréguer et al., 1995; Hendry et al., 2010). These organisms with silica skeletons sequester carbon and hence mediate atmospheric CO_2 through burial (Ragueneau et al., 2000). In addition, weathering of silicate minerals through reaction with carbonic acid (dissolved in meteoric water) also provides a sink for atmospheric CO_2 (Walker et al., 1981). As stable isotope fractionation can provide information about sources and rates in such cycles, the Si isotope system is of obvious relevance to the aforementioned processes.

Over the last decade there have been a number of studies investigating Si isotopes in biological and weathering processes. These have demonstrated that isotopic fractionation is generated as a result of biological utilisation by marine organisms (De La Rocha et al., 1998; Hendry et al., 2010) or vegetation (Ding et al., 2005; Opfergelt et al., 2008; Bern et al., 2010), low-temperature weathering (Ziegler et al., 2005a&b; Georg et al., 2009a; Bern et al., 2010; Opfergelt et al., 2009, 2010, 2011, 2012; Steinhoefel et al., 2011) and precipitation of secondary silica (Basile-Doelsch et al., 2005). Precipitation of secondary minerals tends to enrich the product in the lighter isotopes of Si – compared to unweathered igneous rocks (~ $-0.4 < \delta^{30}Si < -0.1$‰; Savage et al., 2010, 2011, 2012), large negative mineral enrichments of $\delta^{30}Si \approx -6.0$ to -3.0‰ have been deduced (e.g., Basile-Doelsch et al., 2005; Ziegler et al., 2005a&b) – resulting in a fluid with a relatively heavy isotopic composition (De la Rocha et al., 2000; Ding et al., 2004, Georg et al., 2006a, 2009b; Cardinal et al., 2010). This appears to be as a result of dynamic equilibrium between dissolution and re-precipitation of Si, whereby the degree of isotopic fractionation is much greater during the formation of secondary phases than during dissolution

(e.g. Ziegler et al., 2005a). There has, however, been no systematic study of the overall Si isotopic composition of, and the degree of isotopic heterogeneity within, the continental crust. Ultimately, all Si utilised in the above environments is sourced from the continents and so characterising this source is essential.

The widely-cited studies of Douthitt (1982) and Ding et al. (1996) were the first to hint at the isotopic composition of the continental crust but, since then, very little progress has been made. In both studies it was demonstrated that evolved (high-Si) igneous rocks tended to be enriched in the heavier isotopes of Si and were more isotopically variable when compared to basalts and mantle lithologies. Such observations have since been reappraised using modern analytical techniques, but are still broadly accepted (Savage et al., 2010, 2011, 2012). The earlier studies also suggest that chemically derived sedimentary material (e.g., siltstone, shale) is, in general, isotopically lighter, whereas the Si isotopic composition of mechanically derived sediment (e.g., sandstone) is comparable to that of igneous rocks (again, these observations have been corroborated by more recent weathering studies, see above). However, both of these studies were aimed at cataloguing the natural variation of Si isotopes, and no attempt was made to provide an average isotopic composition for the UCC.

This research uses a well-characterised set of shale and loess samples, as well as the data for granitoid material previously acquired (Savage et al., 2012) to characterise the UCC. The degree of Si isotopic heterogeneity in the UCC is also constrained.

2. SAMPLES

2.1 Loess

Loess is aeolian sediment that covers approximately 10% of the world's land surface and is deposited during cold-dry climatic phases (Taylor et al., 1983; Pye, 1995). It is composed mainly of quartz, feldspar, sheet silicates and/or calcite depending on regional geology, and is derived

predominantly from deserts and/or glacial milling (Taylor et al., 1983). Mechanical sedimentary derivation from glacial milling has limited the extent of chemical weathering that has affected loess, although most loess has experienced at least one cycle of chemical alteration (Gallet et al., 1998). Because loess samples large areas of crust, it has been used by many to constrain the average composition of the upper continental crust (e.g., Taylor et al., 1983; Barth et al., 2000; Hu and Gao, 2008). We have analysed 13 Pleistocene loess samples, sourced from China, New Zealand, Germany, Hungary and the USA, which have previously been studied for major and trace elements (Taylor et al., 1983, Gallet et al., 1998, Barth et al., 2000; Hu and Gao, 2008) and Li and Mg stable isotopes (Teng et al., 2004; Li et al., 2010). The major element composition of loess is somewhat variable, with each suite reflecting the diverse regional geology of its source region, e.g., Si-rich loess from the Banks Peninsula is derived from Mesozoic greywackes from the Southern Alps, whereas European loess is more carbonate-rich, reflecting its derivation from Alpine terrains. The Iowa and Kansas loess is thought to derive from the Rocky Mountains; by contrast, much Chinese loess is non-glacial, deriving instead from a desert environment (Taylor et al., 1983).

Degree of chemical weathering of a sediment is often established using the Chemical Index of Alteration (CIA; Nesbitt and Young, 1982) which is defined as CIA = molar Al_2O_3 / [Al_2O_3 + CaO* + Na_2O + K_2O]. In this equation, CaO* refers to the CaO present only in silicates, not in apatite and carbonate, and is corrected using molar P_2O_5 and Na_2O quantities (see McLennan, 1993). The loess samples analysed in this study have CIA values between 57 and 65, which is slightly elevated when compared to unweathered igneous rocks (CIA ~ 50; Nesbitt and Young, 1982), but lower than shales (see later), consistent with the suggestion of Gallet et al. (1998) that most loess has experienced minor chemical weathering.

2.2 Shales

Shales are fine-grained sedimentary rocks composed mainly of clay minerals, detrital quartz,

and variable amounts of carbonate, which are deposited in low energy environments. They are derived from erosion over large areas and so, like loess, are often used as representative samples of the upper continental crust (e.g., Haskin and Haskin, 1966; Nance and Taylor, 1976; Gromet et al., 1984; Taylor and McLennan, 1985; Barth et al., 2000). Shale petrogenesis is more complicated than loess, involving both mechanical and chemical weathering, as well as variable amounts of diagenesis and metamorphism, resulting in higher CIA values than loess. Despite this, shales show little variation in their insoluble element ratios (Taylor and McLennan, 1985) and so provide good estimates for these in the upper crust. Also, whereas loess is normally confined to the Pleistocene, shales are present in the geological record throughout most of Earth's history.

Thirty eight samples, taken from Australia, Canada and the USA were analysed for Si isotopes. Twenty two shales were analysed from the Post-Archaean Australian Shale (PAAS) suite, originally used by Nance and Taylor (1976) to estimate the rare earth element composition of the upper continental crust, and subsequently by Taylor and McLennan (1985), Barth et al. (2000) and Hu and Gao (2008) for further trace element work, and Teng et al. (2004) and Li et al. (2010) for Li and Mg stable isotopes studies, respectively. These samples were collected from across Australia (see Figure 1 in Nance and Taylor, 1976) and span a wide range of ages from mid-Proterozoic (1.5 Ga) to Triassic (200-250 Ma). All samples were taken from drill cores to avoid the effects of weathering and/or leaching. CIA values of the PAAS shales are high and variable, ranging from 66 to 80 (c.f. ~50 for unweathered igneous rocks). As well as the PAAS samples, we have analysed two shales from the Pilbara Supergroup, Western Australia (McLennan et al., 1983), which have Archaean deposition ages of 3.4 Ga (Gorge Creek) and 2.7 Ga (Whim Creek) respectively.

Seven samples were taken from the Huronian Supergroup and Sudbury Basin suites, Canada (McLennan et al., 1979; McDaniel et al., 1994; McLennan et al., 2000). Samples from the Huronian Supergroup are early Proterozoic in age and are composed predominantly of granitoid and volcano-sedimentary material derived from the Archaean-age Superior Province (McLennan et al., 1979). A

slightly younger (1.85 Ga) sandstone from the nearby Sudbury basin (McDaniel et al., 1994), which is again thought to derive from the Superior Province, was also analysed. Some of these samples resemble tillites or glacial mudstones (i.e., the Gowganda samples, see Table 3) that have not experienced large amounts of chemical alteration, as evinced by their lower CIA values. These samples may therefore be more representative of unweathered Archaean continental crust, rather than the more chemically altered shales.

Four metasedimentary samples were analysed from the Honda Group and Uncomphagre Formation in south-western North America (McLennan et al., 1995). These samples represent a quartzite-pelite stable-shelf succession, derived from differentiated Proterozoic-age crust with small but variable amounts (10–25%) of Archaean material. The major element compositions indicate that these samples contain minor carbonate and have undergone severe weathering before deposition (McLennan et al., 1995).

Finally, the USGS shale standards SDO-1, SCo-1 and SGR-1b were also analysed. All of these samples are from the USA and contain varying amounts of carbonate material, with SCo-1 showing the strongest terrestrial affinity. Sample SGR-1b is from an oil shale, which has anomalously low SiO_2 content (< 30 wt. %) and CIA value (36), because this sample is not predominately silicate-derived.

3. METHODS

Samples were prepared for MC-ICPMS analysis following the methods and techniques detailed by Georg et al. (2006b). These are comprehensively described in the aforementioned paper, and elsewhere (e.g., Armytage et al., 2011; Savage et al., 2011; Zambardi and Poitrasson, 2011); as such, only a brief summary and any sample-pertinent information will be provided here. All samples were received as powders, some of which had been milled in agate. It has been demonstrated that this does not cause resolvable contamination for Si isotope analysis (e.g., Savage et al., 2011; Zambardi and

Poitrasson, 2011).

Between 5 and 10 mg of sample powder was weighed into a silver crucible along with ~ 200 mg of NaOH flux (analytical grade in pellet form). The crucible was then placed into a furnace, heated at 720ºC for 12 minutes, then removed and allowed to cool slightly. After fusion, the crucible was placed into 20 ml of MQ-e water in a Teflon beaker, and left to react for 24 hours. Afterwards, the beaker was left in an ultrasonic bath (heated to ~ 60°C) for 20 minutes, then transferred from the crucible via a pipette into pre-cleaned 125 ml PP bottles. Finally, the sample was diluted with MQ-e water and acidified (1% v/v) with triple-distilled HNO_3. Sample yield was then checked using the "Heteropoly Blue" method (whereby Si is measured in the form of a Mo-Si complex) using a Hach Lange DR 2800 photospectrometer. The average yield for all loess and shale samples processed in this study is 96 ± 4 % (2 s.d.).

Samples were quantitatively purified before MC-ICPMS analysis using a single-pass column technique with strong cationic resin (BioRAD AG50W X12, 200-400 mesh, in H^+ form). Silicon, at neutral to low pH, exists in solution as either anionic or neutral species, so it is not retained by the resin. It is therefore eluted immediately in MQ-e water, and all cations are quantitatively stripped from the sample (Georg et al., 2006b). The samples were acidified after purification to 1% v/v HNO_3. All samples and standards, including the bracketing standard, underwent identical chemical processing before analysis, and the external standards BHVO-2 and Diatomite (see Section 4.1) were routinely analysed to assess method accuracy and reproducibility.

There is some evidence that the presence of anionic species (e.g. organic carbon, SO_4^{2-}, NO_3^-) in the eluant can lead to matrix effects on the measured Si isotopic ratios: both van den Boorn et al. (2009) and Hughes et al. (2011) show that high SO_4^{2-}/Si and C/Si ratios can cause substantial shifts in the measured Si isotope composition of various rock standards, including BHVO-2 and SGR-1. Our analyses of both of these standards are identical within error to the recommended, matrix-free, values for these materials (see Table 1), even though we did not employ any further steps to combat matrix

effects. It is highly likely that the alkali fusion step, at 720°C, should act to volatilise and thus remove much of the sulphate and carbon (Savage et al., 2010; Zambardi and Poitrasson, 2011); also it has also been suggested that some MC-ICPMS instrumental setups may be more sensitive to matrix effects than others (Hughes et al., 2011). Nevertheless, the good agreement between our external standard measurements and those provided by van den Boorn et al. (2009) and Hughes et al. (2011) strongly implies that our data are uncompromised by matrix-effects, even for samples such as SGR-1 which have high SO_4^{2-}/Si ratios.

Silicon isotope measurements were made at the University of Oxford on a Nu Instruments (Wrexham, UK) Nu Plasma High Resolution Multi-Collector Inductively-Coupled-Plasma Mass Spectrometer (HR-MC-ICPMS). The machine and running conditions are detailed in Belshaw et al. (1998) and Georg et al. (2006b). The machine was operated at "medium" resolution (resolving power $m/\Delta m \sim 3300$, where Δm is defined at 5% and 95% for peak height; Weyer and Schwieters, 2003) to avoid poly-atomic interferences (e.g., $^{28}Si^{1}H^{+}$, $^{14}N^{16}O^{+}$) that would otherwise prevent the accurate measurement of all three Si isotopes. This entails physically narrowing the ion beam and typically results in a ~ 85% reduction of instrument sensitivity. During the course of this study, typical sample run Si concentrations were between 750 ppb and 1.0 ppm (depending on machine conditions), which gave a total signal of $\sim 1 \times 10^{-10}$A and a signal to noise ratio of ~ 400.

To correct for instrumental mass-bias, Si isotope values were calculated using the standard-sample bracketing technique, with NBS28 (NIST RM8546) silica sand as the bracketing standard. Isotopic variations from this standard are represented in per mil (‰) using the delta notation, defined as:

$$\delta^{30}Si = [(^{30}Si/^{28}Si_{sample})/(^{30}Si/^{28}Si_{standard}) - 1] \times 1000;$$

$$\delta^{29}Si = [(^{29}Si/^{28}Si_{sample})/(^{29}Si/^{28}Si_{standard}) - 1] \times 1000.$$

We discuss our Si isotopic data using $\delta^{30}Si$ values, which are roughly twice the magnitude of $\delta^{29}Si$ values. Assuming mass dependence, which, for terrestrial samples, is a valid assumption, this relationship was used as a further test for data quality, as unresolved isobaric interferences should result in an artificially high abundance of one (or more) of the isotopes of interest.

4. RESULTS

4.1 External standards

The external standards Diatomite (a pure natural silica standard) and BHVO-2 (Hawaiian basalt, USGS) were routinely analysed to assess sample data accuracy and precision. Both are widely available and often utilised; as such, well-established literature data are available for comparison. Also analysed was the USGS SGR-1b oil shale standard, which has also been analysed by Hughes et al. (2011). External standard data are given in Table 1 as well as some reference values (Reynolds et al., 2007; Abraham et al., 2008; Georg et al., 2009a; Hughes et al., 2011; Savage et al., 2011; Zambardi and Poitrasson, 2011). The data for all standards are in excellent agreement with the literature data, and illustrate the good levels of accuracy and reproducibility that our methods can attain. The external reproducibility can be estimated by calculating the 2 s.d. (2 × the standard deviation) of the mean of the individual standard analyses given in Table 1. The averages and 2 s.d. are as follows – Diatomite: $\delta^{30}Si$ = 1.22 ± 0.03 ‰; n = 12; BHVO-2: $\delta^{30}Si$ = -0.30 ± 0.04 ‰; n = 12 – the largest of these values (± 0.04 ‰) is taken to represent the external reproducibility.

Silicon isotope data for the loess and shale samples are given in Tables 2 and 3, respectively. Errors for individual sample analyses are represented by both 2 s.d. and 95% standard error of the mean, calculated as such: 95% s.e. = t × s.d./$(n)^{1/2}$, where t = inverse survival function of the Student's t-test at the 95% significance level and n-1 degrees of freedom; the 95% s.e. values (± 0.01 – 0.05‰; mean ± 0.03 ‰), which are appropriate as one aliquot of each sample was analysed, are similar to our

external precision values calculated above.

4.2 Loess

Loess displays limited variation in Si isotopes, with $\delta^{30}Si$ values ranging from -0.28 to -0.15‰, and an average value of $\delta^{30}Si$ = -0.22 ± 0.07 ‰ (2 s.d., n = 13, Fig. 1). There is some minor isotopic variation between localities, with the European (German and Hungarian) loess samples having slightly heavier $\delta^{30}Si$. However, these variations are within error and there are no resolvable differences between loess derived from distinct continental provinces. There are also no strong correlations with SiO_2 content, weathering degree (CIA values) or other isotope systems (Figs. 2, 3b and 4). This limited isotopic range is in contrast to the $\delta^{26}Mg$ and $\delta^{7}Li$ values of these samples, which display 3× and 60× greater isotopic variability, respectively (Teng et al., 2004; Li et al., 2010).

4.3 Shales

In contrast to the loess data, the PAAS samples define a wider range of $\delta^{30}Si$ values, with samples ranging from $\delta^{30}Si$ = -0.80 to 0.00 ‰ (average $\delta^{30}Si$ = -0.37 ± 0.47 ‰; 2 s.d., n = 22; 2 s.d. is abnormally large because the data are not normally distributed). Compared to igneous rocks (~ -0.4 < $\delta^{30}Si$ < -0.1‰; Savage et al., 2010, 2011, 2012), this is a wide spread of Si isotope compositions although it is somewhat limited compared to the much larger isotope variations measured in secondary minerals and soils (~ -6.0 < $\delta^{30}Si$ < +1.0 ‰; e.g. Basile-Doelsch et al., 2005; Ziegler et al., 2005a&b; Opfergelt et al., 2010, 2011, 2012). Within each locality (with the exception of the Mt. Isa shales) there is remarkably limited Si isotope variation. There are no strong correlations between Si isotopes and SiO_2 (Fig. 2) or Li and Mg stable isotope compositions (Fig. 4), although there is a scattered negative trend (R^2 = 0.14) with CIA values (Fig. 3a). The two Archaean-age Pilbara shales from Australia are both isotopically much lighter than igneous rocks (sample Pg-7 displays the lightest $\delta^{30}Si$ value analysed in this study, viz. -0.82 ± 0.04 ‰, 95% s.e.), and show similar isotopic compositions to some

of the younger PAAS samples. The data for the SW USA shales (Honda and Uncomphagre) also show a limited range ($\delta^{30}Si$ = -0.51 to -0.40 ‰, average $\delta^{30}Si$ = -0.47 ± 0.10 ‰; 2 s.d., n = 4), again lighter than the range for igneous rocks.

Silicon isotope data for the Canadian samples (Huronian and Sudbury) range from $\delta^{30}Si$ = -0.41 to -0.16 ‰ (average $\delta^{30}Si$ = -0.25 ± 0.20 ‰; 2 s.d., n = 7). The range of Si isotopic compositions is smaller than for the PAAS samples, with the data falling into two populations; one near $\delta^{30}Si$ = -0.39 ‰, the other around $\delta^{30}Si$ = -0.19 ‰, the possible causes of which will be discussed later.

The USGS standards are geologically unrelated, with varied petrogenetic histories and ages. The $\delta^{30}Si$ data lie within the range defined by PAAS shales. Sample SGR-1b, an organic-rich oil-shale, has a relatively heavy Si isotopic composition ($\delta^{30}Si$ = +0.01 ± 0.04 ‰, 2 s.d.); this could indicate the presence of biogenic silica, which is typically isotopically heavy compared to terrestrial silicate material (e.g., De la Rocha et al., 1998; Opfergelt et al., 2008; Hendry et al., 2010).

5. DISCUSSION

The data described above show that, with respect to Si isotopes, the UCC is heterogeneous relative to the mantle and igneous rocks (Savage et al., 2010, 2011, 2012). The following discussion concerns how these data can be used to constrain the Si isotopic composition of the modern day UCC, as well as interpreting the Si isotope composition of clastic sedimentary material in terms of what is already known about possible sources and Si isotope fractionation as a result of low temperature, critical zone, processes. These results will then be combined with data from other sources to calculate an average UCC Si isotopic composition.

5.1 Loess as a proxy for the composition of the UCC

The differences in isotopic heterogeneity between loess and shales reflect the different

petrogenetic histories of these two lithologies. The consistency of the Si isotopic composition of loess from all over the globe is remarkable. Not only is the range of loess $\delta^{30}Si$ limited with respect to shale samples, it is also smaller than the isotopic range displayed by igneous rocks (Fig. 1). This is despite loess sampling a wide range of lithologies (Taylor et al., 1983), exhibiting a broad range of chemical compositions (SiO_2 content ranging from 52 to 81 wt.%, with the high SiO_2 in some loess reflecting concentration of quartz; Fig 2), and having, in general, experienced at least one cycle of chemical weathering (Gallet et al., 1998). Finally, these same loess samples show resolvable (and in some cases, quite large) variations in their $\delta^{7}Li$ and $\delta^{26}Mg$ values, which in both cases are related to weathering processes (Fig. 4; Teng et al., 2004; Li et al., 2010). Why then, is the Si isotopic composition of loess so consistent, when chemical weathering has been shown to generate resolvable Si isotopic fractionation?

The most likely explanation for this can be found by taking into account the mineralogy of loess, in which the most common Si-bearing phases are quartz and feldspar, i.e., primary igneous minerals (Pye, 1995). Even though loess has undergone weathering, Si isotopes should only be affected if there has been significant formation of secondary mineral phases. This is not so for the CIA value, which is a proxy for loss of fluid-mobile elements (Ca, Na and K) with respect to Al, predominantly due to breakdown of primary feldspar. Even though Si is more water-soluble than Al (at acidic to neutral conditions; $2 < pH < 8$), it is much less so than Ca, Na and K (Turner et al., 1980) and increases in CIA value recorded by loess should not necessarily imply any significant Si loss from the bulk rock. On the other hand, Mg and Li isotopes are a) both strongly fluid mobile and b) not present in large amounts in either quartz or feldspar, and are therefore more amenable to secondary weathering effects.

The average Si isotope value for loess is $\delta^{30}Si = -0.22 \pm 0.07$ ‰ (2 s.d., n = 13). The major Si-bearing phases in loess are quartz and feldspar, therefore loess is likely behaving as a proxy for the composition of average quartz and feldspar in the UCC. We refer to this as “fresh crystalline” UCC and it is identical to the average value for granites ($\delta^{30}Si = -0.23 \pm 0.15$ ‰; 2 s.d.; Savage et al., 2012) and

also the average “igneous” value for the continental crust, calculated from the empirical igneous array in Savage et al. (2011; $\delta^{30}Si$ = -0.23 ± 0.05 ‰; 2 s.e. of the regression statistics).

The Canadian (Huronian and Sudbury) sediments define two Si isotope populations (Fig. 1), which appear to be related to weathering degree, with the more isotopically negative group displaying higher CIA values (Fig. 3). The samples with heavier Si isotopic compositions have CIA values comparable to loess (Fig. 3b) and are thought to be glaciogenic (McLennan et al., 1979), i.e., they formed via predominantly mechanical processes, similar to loess. If loess is taken to represent the Si isotopic composition of crystalline modern day continental crust, then the low-CIA samples from the Huronian and Sudbury basins should record the same reservoir at the time given by their deposition ages, in this case between 2.2 and 2.5 Ga (McLennan et al., 2000). The average Si isotope composition for these samples is $\delta^{30}Si$ = -0.19 ± 0.05 ‰ (2 s.d.), identical within error to that given by modern day loess ($\delta^{30}Si$ = -0.22 ± 0.07 ‰). This is good, if modest, evidence that the Si isotopic composition of crystalline upper continental crust has remained constant since at least 2.5 Ga. It is, however, difficult to place conclusive limits on the basis of six samples from two localities, and it is not clear whether a different melting regime at subduction zones before ca. 2.5. Ga (e.g., Taylor and McLennan, 1985; Martin, 1986; Kemp and Hawkesworth, 2003) might have affected the Si isotopic composition of bulk continental crust formed at this time.

The more isotopically negative shale samples from the Canadian suite, the Pilbara suite and from SW USA are all derived from Archaean or Palaeo-proterozoic terrains, and were also deposited during these geological periods. This implies that the UCC was as heterogeneous then, with respect to Si isotopes, as it is today.

5.2 The formation of shales

If loess represents the average Si isotopic composition of the crystalline UCC, then the more variable isotopic compositions in shales illustrate the effect that geological processes at the Earth's

surface have on Si isotopes, in particular, weathering and the sedimentary cycle. The effect of weathering on Si isotopes is now well established, through studies of natural soil and clay formation as well as studies of riverine Si and associated bedrock (Section 1) as well as some experimental work (Ziegler et al, 2005a; Delstanche et al., 2009). These studies have established that precipitation of Si from solution enriches the product (e.g., secondary mineral phases) in the light isotopes of Si, leaving an isotopically heavy fluid.

Given that shales are composed of significant quantities of clay minerals, do the Si isotopic compositions of shales reflect their mineralogy? Certainly, some samples do display light δ^{30}Si values (i.e., Perth Basin, Pilbara) and the mean δ^{30}Si value for shales is lighter than for loess. However, there are some shales that have δ^{30}Si values that are similar to igneous material and, also, some samples that display Si isotopic compositions that are *heavier* than unweathered continental crust (i.e., the Mt. Isa group). Also, given the large (per mil) enrichments in light Si isotopes recorded in many secondary phases, particularly in clay minerals (e.g. Opfergelt et al., 2012), it is somewhat surprising that the Si isotopic variations recorded in shales are limited to the sub-per mil scale.

It appears that the presence of secondary phases does not always cause a shift towards light Si isotope compositions in shales. The poor relationships between δ^{30}Si and CIA values (Fig. 3a) and Li and Mg isotopic compositions (Fig. 4) might serve to illustrate this; however, as noted for the loess samples, these quantities are not indicative of Si mobility during weathering. This is due to, in part, the lower fluid mobility of Si compared to Li, Mg, Ca etc., and also the fact that Si is present in significant quantities in both primary and secondary silicate minerals – therefore, the δ^{30}Si of a shale is likely strongly controlled by the relative abundances of these two mineral groups, which in turn depends on the degree of weathering a sedimentary source has undergone.

Weathering of upper crustal material can be divided into three stages (Chesworth, 1977; Kronberg et al., 1979). “Early stage” weathered material is dominated by primary minerals (that is, minerals that constitute fresh igneous or metamorphic lithologies) with a clay fraction consisting of

chlorite, vermiculite, smectite and illite. Loess is a good example of "early stage" weathering (e.g. Pye, 1995). "Intermediate stage" weathered material typically contains detrital quartz and a clay fraction predominately composed of smectite and illite (2:1 clays – one octahedral hydroxide "sheet" per two tetrahedral silicate "sheets"), accompanied by loss of feldspar. "Late stage" material is dominated by the quartz-kaolinite (1:1 clays – one hydroxide to one silicate "sheet")–gibbsite-goethite assemblages.

Shales typically have intermediate to late-stage mineralogies, where feldspar has been completely replaced by clay minerals but detrital quartz is still modally significant. Clay minerals are isotopically much lighter than primary feldspars but quartz will have a heavier Si isotopic composition, which will serve to dilute the strongly fractionated clay mineral signature, depending on the detrital quartz abundance. Also, the type of clay minerals present in the shale is likely to exert a control on the bulk Si isotope composition: there is now strong evidence that formation of more mature (more desilicified) 1:1 clays is accompanied by much larger degrees of Si isotopic fractionation than 2:1 clays, with kaolinite displaying the most negative δ^{30}Si values (Georg et al., 2009a; Opfergelt et al., 2012). During "late stage" alteration, an isotopic shift to lighter values associated with kaolinite formation could also be compounded by the associated formation of Fe oxides, as sorption of Si on to Fe-oxides also results in an enrichment of light Si isotopes (Delstanche et al., 2009; Opfergelt et al., 2009). Therefore, quantifying the amount of primary Si remaining (that is, the amount of desilicification that a shale has undergone) as well as the variety of clay minerals present may be more useful for quantifying shale Si isotopic compositions.

One way to assess this is to study the relationship between Si isotopes and Al/Si ratios, and insoluble element concentrations, such as the rare earth elements (REEs), Nb, Ti, etc. An increased abundance of 1:1 clays in a sample should correspond to a higher Al/Si ratio, and also, because of progressive chemical denudation, insoluble element concentrations (Duddy, 1980). Laterite formation, for example, which involves intense degrees of weathering, can significantly concentrate the REEs (Kronberg et al., 1979) and would be predicted to result in light Si isotope compositions, due to the

387 significant abundances of kaolinite and Fe-oxides in laterites. It is striking, therefore, that negative
388 correlations do exist between Si isotope composition and Al/Si ratios as well as insoluble element
389 concentrations in shales, for instance TiO_2 (R^2 = 0.41), Ho (R^2 = 0.45), Hf (R^2 = 0.55 – not including
390 loess, which show evidence of zircon accumulation; Taylor et al., 1983). The examples of Al/Si and
391 Nb are shown in Figure 5. These relationships indicate that the shales that display the largest
392 enrichment in Al/Si ratios (i.e. have higher kaolinite abundances) and insoluble elements (i.e., have the
393 lowest Si_{qtz} contents) tend to have the lightest Si isotope compositions compared to igneous crust (e.g.,
394 Pilbara, Perth Basin). Those shales with Al/Si and insoluble element compositions close to average
395 upper crust also have Si isotope compositions similar to igneous upper crust (e.g., State Circle). All
396 shales show similar depletions of fluid-mobile elements as a result of feldspar breakdown (recorded by
397 their CIA values), but in samples enriched in the insoluble elements, alteration has been more intense or
398 involved reworking of already-weathered sediment – enough to induce negative shifts in Si isotope
399 composition. Another outcome of the relationship between Si isotopes and insoluble element
400 concentrations is that it offers a possible explanation for the relatively heavy Si isotopic compositions
401 in some shales. Taylor and McLennan (1985) noted that shales with low REE content contain a
402 significant quantity of marine-derived material. The concentration of rare earth elements in seawater is
403 low because they are extremely particle reactive, so are removed from the water column by scavenging
404 (e.g. Elderfield, 1988; Halliday et al., 1992). This is reflected in the REE content of carbonates and
405 other marine lithologies, including cherts and siliceous ooze. Seawater also has a heavy Si isotope
406 composition (De La Rocha et al., 2000), and so seawater derived authigenic silica is also relatively
407 heavy, compared to igneous rocks (De la Rocha et al., 1998; Hendry et al., 2010; also cf. Diatomite
408 standard). Therefore, if a sediment is predominantly marine, then it will have low insoluble element
409 concentrations, low Al/Si ratios and heavy Si isotope compositions, which can explain the deviation
410 toward heavier Si isotopes in Figure 5. In this regard, it is worth noting that the isotopically heavy Mt.
411 Isa Group has chert, dolomite and carbonate horizons and contains stromatolites and halite

412 pseudomorphs (Geoscience Australia; http://dbforms.ga.gov.au).

413 An important aspect to stress is that the processes that control the Si isotopic composition of
414 shales, namely intensive weathering and addition of marine-derived silica, are not mutually exclusive.
415 Mixing between these two end-members could result in a Si isotopic composition that is unfractionated
416 with respect to igneous rocks, masking the various isotopically fractionated components of such a
417 sample

418 This is illustrated in Figure 6, where we have modelled the various sedimentary components
419 and processes in shales (and loess), in terms of their $\delta^{30}Si$ and Al/Si values. The starting material is
420 granitic, composed of 60% feldspar ($\delta^{30}Si$ = -0.30‰) and 40% quartz ($\delta^{30}Si$ = -0.20‰; mineral $\delta^{30}Si$
421 based on analyses in Savage et al., 2012), which gives an initial composition of $\delta^{30}Si$ = -0.25‰, Al/Si =
422 0.25 (star symbol in Fig. 6). The simplest scenario in Figure 6 is feldspar dissolution, or quartz
423 accumulation, illustrated by line A. This lowers the Al/Si ratio but barely affects $\delta^{30}Si$, and fits the loess
424 data well, illustrating the strong control that primary igneous minerals have on the Si isotope
425 composition of loess (Section 5.1).

426 Scenarios B and C in Figure 6 both illustrate secondary mineral formation, whereby feldspar is
427 gradually replaced by 2:1 smectite clay ($\delta^{30}Si$ = -1.1‰, Al/Si = 0.67) or 1:1 kaolinite clay ($\delta^{30}Si$ = -
428 2.0‰, Al/Si = 1; clay mineral $\delta^{30}Si$ taken from Opfergelt et al., 2012). In both scenarios there is also a
429 reduction in the abundance of detrital quartz. Where smectite is replacing feldspar and there has been
430 25% reduction of detrital quartz (scenario B), the most negative predicted value is $\delta^{30}Si$ = -0.63‰.
431 Whilst this minimum can account for many of the shale Si isotope compositions, it fails to model many
432 of the Al/Si ratios well. Scenario C, in which kaolinite is forming at the expense of feldspar, and there
433 is a much large (60%) remobilisation of detrital quartz, fits the shale data to a better degree. In this
434 instance, the most negative shale samples can be explained by 70% replacement of the feldspar by
435 clays, and a loss of ~45% of the original quartz; in other words, these shales have
436 quartz:feldspar:kaolinite abundances of ~ 0.3:0.2:0.5. In reality it is unlikely that feldspar is present at

all in shale, but this serves to illustrate that kaolinite appears to be an important phase in creating the lightest Si isotope compositions in shales. It is also highly unlikely that a shale will be sourced from a single lithology and this is illustrated by the horizontal deviations from the linear array in Figure 6; an offset towards lower Al/Si implies accumulation of quartz, an offset toward higher Al/Si implies accumulation of clay minerals.

A final component in the system is that of authigenic marine silica, as shown by scenario D. This describes simple mixing between the granitic starting composition and the Diatomite standard ($\delta^{30}Si$ = +1.24‰, Al/Si = 0) and shows that, for example, only ~10% incorporation of this highly fractionated material is needed to explain the heavier Si isotope compositions of the Mt. Isa group shales. This could be a conservative estimate, as Diatomite is by no means the most fractionated authigenic material measured in the literature, with some stromatolitic samples display Si isotope compositions of > 3‰ (Hendry et al., 2010; Wille et al., 2010). This also assumes that the starting material is unweathered – a shale with both high kaolinite and biogenic silica content could have a loess-like Si isotope composition, because weathering and addition of biogenic silica are antithetic (and sub-parallel, see Fig. 6). Other proxies are required to tease out the relative contributions of terrestrial and authigenic marine silica to a shale if, for instance, negative Si isotope deviations from "igneous" were to be used as a proxy for degree of large-scale terrestrial weathering. One possibility could be the use of Ge/Si ratios which are markedly different between biogenic and secondary silicate phases (e.g. Derry et al., 2005; Cornelis et al., 2011), but the Ge data for the samples used in this study, if present, are of too poor precision to infer any relationship.

It is clear that the Si isotope composition of shales is both source and process-related. Although it is very difficult to identify one major control, it appears that the balance of primary vs. secondary minerals (in particular, detrital quartz and kaolinite) is important. This degree of homogenisation is the reason why shales have been so useful, in previous studies, for constraining average UCC, and should provide a more representative upper crustal Si isotopic composition.

462

463 **5.3 The silicon isotope composition of the upper continental crust**

464 The upper continental crust consists predominantly of sedimentary and felsic igneous
465 lithologies (or their metamorphosed analogues; Wedepohl, 1995) and so by combining the data
466 acquired during this study with that for granitoid material (Savage et al., 2012), one may characterise
467 the Si isotopic composition of the UCC. These data are shown in histogram form in Figure 7. The
468 distribution is non-Gaussian when the shales are included, which reflects the greater variability and
469 more stochastic nature of the shale Si isotope compositions. A fairly sharp peak is centred around δ^{30}Si
470 ~ -0.25 to -0.20 ‰ and is defined primarily by the granite and loess data, with the shale data defining
471 much larger and relatively even spread of Si isotope compositions.

472 The UCC is much more heterogeneous than the mantle or oceanic crust, with respect to Si
473 isotopes (Fig. 1). This heterogeneity is displayed by the shale samples, which reflect long-term and/or
474 intense chemical weathering processes, and also, the presence of marine-derived sedimentary material
475 that is now part of the continental crust. The granites define a more reduced range, but do show more
476 variability than their extrusive counterparts (rhyolites and dacites samples that show no evidence for an
477 evolved source during petrogenesis; Savage et al., 2011), likely to be the result of sediment anatexis
478 during granite petrogenesis (Savage et al., 2012). The loess define the narrowest range of Si isotopic
479 compositions, likely due to the fact that loess mineralogy is dominated by primary igneous silicates
480 (see Section 5.1). The overriding "igneous" affinity of loess is demonstrated by the fact that the average
481 value for loess (δ^{30}Si = -0.22 ± 0.07 ‰) is identical to that of granites (δ^{30}Si = -0.23 ± 0.15 ‰) and
482 indicates that the average loess value is a good proxy for the Si isotope composition of fresh crystalline
483 upper continental crust.

484 A more robust isotopic average for the upper continental crust requires an estimate of the
485 average proportions and SiO_2 compositions of the various lithologies that comprise the UCC. Using the
486 study of Wedepohl (1995), four major units can be defined, along with their average SiO_2 contents as

follows (Table 4): sedimentary lithologies (14%; SiO_2 = 52.4 wt.%); felsic intrusive lithologies (50%; SiO_2 = 69.2 wt.%); gabbros (6%; SiO_2 = 50.1 wt.%); metamorphic lithologies (30%; SiO_2 = 63.7 wt.%). The average $\delta^{30}Si$ value for each of these units can then be calculated and used to derive a weighted UCC Si isotopic composition. Note that the estimates of Wedepohl (1995) give a UCC SiO_2 content of 64.1 wt.%; this value has been superseded by a slightly higher value of 66.6 wt.% (Rudnick and Gao, 2003), but recasting the data using this estimate does not affect the final outcome of the calculation. In the following discussion, all errors are quoted to 2 s.d.

Using data from previous work, the granite average of $\delta^{30}Si$ = -0.23 ± 0.15 ‰ (Savage et al., 2012) is used as an estimate for felsic volcanic rock, and, because there is insignificant Si isotopic variation in mantle-derived igneous rocks (Savage et al., 2010), the BSE value of $\delta^{30}Si$ = -0.29 ± 0.08 ‰ is used to represent gabbro.

The greater degree of isotopic heterogeneity means that calculating a meaningful and reliable average $\delta^{30}Si$ value for the sedimentary unit is more complicated. Firstly, four sub-units are defined (shales and siltstones, sandstones, mafic volcano-clastic sediments and carbonates; Table 4), again following the study of Wedepohl (1995). Silica contents of the sub-units are then calculated using the SiO_2 averages of the samples analysed in this study, or, in the case of mafic volcano-clastic sediments and carbonates sub-units, estimated from other studies. This approach yields an average unit composition of SiO_2 = 52.6 wt.%, which is almost identical to that given by Wedepohl (1995). The average $\delta^{30}Si$ value of all the shale samples analysed in this study is -0.36 ± 0.44 ‰, and this value was used to represent the shale and siltstone sub-unit. The average loess $\delta^{30}Si$ value of -0.22 ± 0.07 ‰ is used to represent the sandstone sub-unit because they are mineralogically similar, at least in terms of the major Si-hosting phases. The BSE average is used to represent mafic volcanoclastic sedimentary material, as with the gabbro unit. The carbonates were assumed to contain negligible amounts of Si, and so are disregarded in the calculation (the final sedimentary $\delta^{30}Si$ value does not alter significantly even if the carbonate unit were to contain 10 wt.% SiO_2 with a $\delta^{30}Si$ value of +1.00 ‰, due to the small

relative proportion of this unit). The above approach yields an average sedimentary unit $\delta^{30}Si$ value of -0.31 ± 0.26 ‰.

To calculate an average $\delta^{30}Si$ value for the metamorphic unit, it is first assumed that this unit contains lithologies that have protoliths present in similar proportions to those in the unmetamorphosed portion of the upper continental crust, because the average SiO_2 composition of this unit is very similar to that of the UCC (Table 4). Metamorphism does not appear to affect the bulk Si isotopic composition of a sample (André et al., 2006), such that the $\delta^{30}Si$ value of this unit should be the weighted average of the sedimentary, felsic and gabbroic units. Alternatively, removing the metamorphic unit from the equation will not affect the final UCC $\delta^{30}Si$ value.

Using the above estimates, the average Si isotopic value of the upper continental crust is calculated to be $\delta^{30}Si$ = -0.25 ± 0.16 ‰ (2 s.d. propagated error from the isotope compositions only; including uncertainties associated with lithological unit abundances and their respective Si contents does not introduce further significant uncertainty). This value coincides with the peak illustrated in Figure 7. Strikingly, this value is only slightly heavier than, but within error of, the value for BSE. Given that chemical weathering fractionates Si isotopes to a relatively large degree, this similarity is perhaps surprising, but is easily explained by the fact that shales and siltstones comprise ~6 wt.% of the UCC, such that these larger variations are effectively masked by the more abundant igneous material (Wedepohl, 1995). The slight overall enrichment in heavier Si isotopes relative to BSE reflects the predominance of felsic lithologies in the upper crust, which have relatively heavier Si isotopic compositions. However, despite the larger spread of data for the UCC relative to BSE, these compositions are identical within uncertainty, which reflects the competing nature of the different sources of Si: igneous differentiation causes a slight enrichment in the heavy Si isotopes, but chemical weathering counteracts this by readily enriching secondary minerals in the lighter isotopes. Furthermore, addition of marine-derived, authigenic, silica to clastic sediments through orogenesis introduces a heavy Si isotope source, which was previously released from the continents via chemical

537 weathering.

538

539 **6. CONCLUSIONS**

540

541 Pleistocene loess samples define a narrow range of Si isotopic compositions (δ^{30}Si = -0.28 to -
542 0.15 ‰), a result of their primary igneous mineralogy and predominantly mechanical weathering
543 history, coupled with the averaging inherent in glaciogenic sampling. The average Si isotopic
544 composition of loess is δ^{30}Si =-0.22 ± 0.07 ‰ (2 s.d.), which is identical to the average Si isotope
545 composition of granites (Savage et al., 2012), and also the δ^{30}Si value calculated for continental crust
546 using the "igneous array" (Savage et al., 2011). This suggests that loess represents the Si isotopic
547 composition of fresh (crystalline) continental crust.

548 Compared to loess, the Si isotopic compositions of shales are much more variable (δ^{30}Si = -0.82
549 to +0.00 ‰) which is a result of a more complicated petrogenesis that can involve, for instance,
550 chemical and physical weathering, diagenesis, etc. as well as variable source lithologies. The average
551 Si isotopic composition of shale (δ^{30}Si = -0.36 ± 0.44 ‰; 2 s.d.) is lighter than loess, due to increased
552 secondary mineral content.

553 Shales are not always isotopically light compared to unweathered igneous material, despite the
554 presence of secondary phases, and Si isotopes in shales do not correlate well with the canonical proxies
555 for weathering, such as CIA values. Instead, good negative correlations between δ^{30}Si values and Al/Si
556 ratios, insoluble element concentrations indicate that more intensive or prolonged chemical weathering
557 of a sedimentary source is required before resolvable negative Si isotopic fractionation occurs. In the
558 absence of marine-derived silica, the δ^{30}Si of a shale sample is a function of the abundance of detrital
559 quartz and the abundance and Si isotopic composition of the secondary phases in that sample. Heavy Si
560 isotopic compositions in shales relative to igneous rocks most likely indicate the presence of marine-
561 derived silica, either by reworking of marine lithologies or deposition in a marine environment.

562 The upper continental crust is heterogeneous with respect to Si isotopes (δ^{30}Si = -0.82 to
563 +0.00 ‰) and has a weighted average composition of δ^{30}Si = -0.25 ± 0.16 ‰ (2 s.d.), which is only
564 slightly heavier than, but statistically identical to, the Bulk Silicate Earth.
565
566 *Acknowledgements:* This study was made possible by the kind donation of samples from Scott
567 McLennan and Roberta Rudnick, and we are extremely grateful for their generosity and, also, their
568 willingness to help with comments on early versions of this manuscript. We would also like to thank
569 Ros Armytage, Julie Prytulak, Kevin Burton, David Pyle and Klaus Mezger for insightful discussion
570 and suggestions along the way. Associate Editor Derek Vance, Wang-Ye Li and two anonymous
571 reviewers provided perceptive and astute reviews that greatly improved this manuscript. Finally,
572 analysis of Si isotopes at Oxford was made possible by the technical support of Steve Wyatt, Nick
573 Belshaw and Teo Krastev. This work was funded by a NERC CASE studentship supported by Nu
574 Instruments and an ERC grant to ANH.

REFERENCES

Abraham K., Opfergelt S., Fripiat F., Cavagna A., de Jong J. T. M., Foley S. F., André L. and Cardinal D. (2008) δ^{30}Si and δ^{29}Si Determinations on USGS BHVO-1 and BHVO-2 Reference Materials with a New Configuration on a Nu Plasma Multi-Collector ICP-MS. *Geostand. Geoanal. Res.* **32,** 193-202.

André L., Cardinal D., Alleman L. Y. and Moorbath S. (2006) Silicon isotopes in ~3.8 Ga West Greenland rocks as clues to the Eoarchaean supracrustal Si cycle. *Earth Planet. Sci. Lett.* **245,** 162-173

Armytage R. M. G., Georg R. B., Savage P. S., Williams H. M. and Halliday A. N. (2011) Silicon isotopes in meteorites and planetary core formation. *Geochim. Cosmochim. Acta* **75,** 3662-3676.

Barth M. G., McDonough W. F. and Rudnick R. L. (2000) Tracking the budget of Nb and Ta in the continental crust. *Chem. Geol.* **165,** 197-213.

Basile-Doelsch I., Meunier J. D. and Parron C. (2005) Another continental pool in the terrestrial silicon cycle. *Nature* **433,** 399-402.

Belshaw N. S., Freedman P. A., O'Nions R. K., Frank M. and Guo Y. (1998) A new variable dispersion double-focusing plasma mass spectrometer with performance illustrated for Pb isotopes. *Int. J. Mass Spectrom.* **181,** 51-58.

Bern C. R., Brzezinski M. A., Beucher C., Ziegler K. and Chadwick O. A. (2010) Weathering, dust, and biocycling effects on soil silicon isotope ratios. *Geochim. Cosmochim. Acta* **74,** 876-889.

Cardinal D., Gaillardet J., Hughes H. J., Opfergelt S. and André L. (2010) Contrasting silicon isotope signatures in rivers from the Congo basin and the specific behaviour of organic-rich waters. *Geophys. Res. Lett.* **37,** L12403.

Chesworth W. (1977) Weathering stages of the common igneous rocks, index minerals and mineral assemblages at the surface of the earth. *J. Soil Sci.* **28,** 490-497.

Cornelis J.-T, Delvaux B., Georg R. B., Lucas Y., Ranger J., and Opfergelt S. (2011) Tracing the origin

of dissolved silicon transferred from various soil-plant systems towards rivers: a review. *Biogeosciences*, **8**, 89–112.

De La Rocha C. L., Brzezinski M. A., DeNiro M. J. and Shemesh A. (1998) Silicon-isotope composition of diatoms as an indicator of past oceanic change. *Nature* **395,** 680-683.

De La Rocha C. L., Brzezinski M. A. and DeNiro M. J. (2000) A first look at the distribution of the stable isotopes of silicon in natural waters. *Geochim. Cosmochim. Acta* **64,** 2467-2477.

Delstanche S., Opfergelt S., Cardinal D., Elsass F., André L. and Delvaux B. (2009) Silicon isotopic fractionation during adsorption of aqueous monosilicic acid onto iron oxide. *Geochim. Cosmochim. Acta* **73,** 923-934.

Derry L. A., Kurtz A. C., Ziegler K. and Chadwick O. A. (2005) Biological control of terrestrial silica cycling and export fluxes to watersheds. *Nature* **433,** 728–730

Ding T., Jiang S., Wan D., Li Y., Li J., Song H., Liu Z. and Yao X. (1996) *Silicon Isotope Geochemistry.* Geological Publishing House, Beijing, China.

Ding T., Wan D., Wang C. and Zhang F. (2004) Silicon isotope compositions of dissolved silicon and suspended matter in the Yangtze River, China. *Geochim. Cosmochim. Acta* **68,** 205-216.

Ding T. P., Ma G. R., Shui M. X., Wan D. F. and Li R. H. (2005) Silicon isotope study on rice plants from the Zhejiang province, China. *Chem. Geol.* **218,** 41-50.

Douthitt C. B. (1982) The geochemistry of the stable isotopes of silicon. *Geochim. Cosmochim. Acta* **46,** 1449-1458.

Duddy L. R. (1980) Redistribution and fractionation of rare-earth and other elements in a weathering profile. *Chem. Geol.* **30,** 363-381.

Elderfield H. (1988) The oceanic chemistry of the rare-earth elements. *Philos. T. R. Soc.-A* **325**, 105-126.

Gallet S., Jahn B., Van Vliet Lanoë B., Dia A. and Rossello E. (1998) Loess geochemistry and its implications for particle origin and composition of the upper continental crust. *Earth Planet. Sci. Lett.* **156,** 157-172.

627 Georg R. B., Reynolds B. C., Frank M. and Halliday A. N. (2006a) Mechanisms controlling the silicon
628 isotopic compositions of river waters. *Earth Planet. Sci. Lett.* **249,** 290-306.

629 Georg R. B., Reynolds B. C., Frank M. and Halliday A. N. (2006b) New sample preparation techniques
630 for the determination of Si isotopic compositions using MC-ICPMS. *Chem. Geol.* **235,** 95-104.

631 Georg R. B., Zhu C., Reynolds B. C. and Halliday A. N. (2009a) Stable silicon isotopes of
632 groundwater, feldspars, and clay coatings in the Navajo Sandstone aquifer, Black Mesa, Arizona,
633 USA. *Geochim. Cosmochim. Acta* **73,** 2229-2241.

634 Georg R. B., West A. J., Basu A. R. and Halliday A. N. (2009b) Silicon fluxes and isotope composition
635 of direct groundwater discharge into the Bay of Bengal and the effect on the global ocean silicon
636 isotope budget. *Earth Planet. Sci. Lett.* **283,** 67-74.

637 Gromet, L P, Dymek, R.F., Haskin, L.A., and Korotev, R.L. (1984) The "North American shale
638 composite": Its compilation, major and trace element characteristics. *Geochim. Cosmochim. Acta*,
639 **48**, 2469-2482

640 Halliday, A.N., Davidson, J.P., Holden, P.E., Owen, R.M. and Olivarez, A.M. (1992) Metalliferous
641 sediments and the scavenging residence time of Nd near hydrothermal vents. *Geophys. Res. Lett.*, **19,**
642 761-764.

643 Haskin M. A. and Haskin L. A. (1966) Rare earths in European shales: a redetermination. *Science* **154**,
644 507–509.

645 Hendry K. R., Georg R. B., Rickaby R. E. M., Robinson L. F. and Halliday A. N. (2010) Deep ocean
646 nutrients during the Last Glacial Maximum deduced from sponge silicon isotopic compositions.
647 *Earth Planet. Sci. Lett.* **292,** 290-300.

648 Hu Z. and Gao S. (2008) Upper crustal abundances of trace elements: A revision and update. *Chem.*
649 *Geol.* **253,** 205-221.

650 Hughes H.J., Delvigne C., Korntheuer M., de Jong J., André L. and Cardinal D. (2011) Controlling the
651 mass bias introduced by anionic and organic matrices in silicon isotopic measurements by MC-
652 ICP-MS. *J. Anal. At. Spectrom.* **26**, 1892-1896

653 Kemp A. I. S. and Hawkesworth C. J. (2003) Granitic perspectives on the generation and secular

654 evolution of the continental crust. *Treatise on Geochemistry* **3,** 349-410.

655 Kronberg B. I., Fyfe W. S., Leonardos Jr. O. H. and Santos A. M. (1979) The chemistry of some
656 Brazilian soils: Element mobility during intense weathering. *Chem. Geol.* **24,** 211-229.

657 Li W., Teng F-Z., Ke S., Rudnick R. L., Gao S., Wu F. and Chappell B. W. (2010) Heterogeneous
658 magnesium isotopic composition of the upper continental crust. *Geochim. Cosmochim. Acta* **74,**
659 6867-6884.

660 Martin H. (1986) Effect of steeper Archean geothermal gradient on geochemistry of subduction-zone
661 magmas. *Geology* **14,** 753-756.

662 McDaniel D. K., Hemming S. R., McLennan S. M. and Hanson G. N. (1994) Petrographic,
663 geochemical, and isotopic constraints on the provenance of the early Proterozoic Chelmsford
664 Formation, Sudbury Basin, Ontario. *J. Sed. Res. A* **64 A,** 362-372.

665 McLennan S. M. (1993) Weathering and global denudation. *J. Geol.* **101,** 295-303.

666 McLennan S. M., Fryer B. J. and Young G. M. (1979) Rare earth elements in Huronian (Lower
667 Proterozoic) sedimentary rocks: Composition and evolution of the post-Kenoran upper crust.
668 *Geochim. Cosmochim. Acta* **43,** 375-388.

669 McLennan S. M., Taylor S. R. and Eriksson K. A. (1983) Geochemistry of Archean shales from the
670 Pilbara Supergroup, Western Australia. *Geochim. Cosmochim. Acta* **47,** 1211-1222.

671 McLennan S. M., Hemming S. R., Taylor S. R. and Eriksson K. A. (1995) Early Proterozoic crustal
672 evolution: Geochemical and Nd-Pb isotopic evidence from metasedimentary rocks, southwestern
673 North America. *Geochim. Cosmochim. Acta* **59,** 1153-1177.

674 McLennan S. M., Simonetti A. and Goldstein S. L. (2000) Nd and Pb isotopic evidence for provenance
675 and post-depositional alteration of the Paleoproterozoic Huronian Supergroup, Canada.
676 *Precambrian Res.* **102,** 263-278.

677 Nance W. B. and Taylor S. R. (1976) Rare earth element patterns and crustal evolution-I. Australian
678 post-Archean sedimentary rocks. *Geochim. Cosmochim. Acta* **40,** 1539-1551.

679 Nesbitt H. W. and Young G. M. (1982) Early proterozoic climates and plate motions inferred from

major element chemistry of lutites. *Nature* **299,** 715-717.

Opfergelt S., Delvaux B., André L. and Cardinal D. (2008) Plant silicon isotopic signature might reflect soil weathering degree. *Biogeochemistry* **91,** 163-175.

Opfergelt S., de Bournonville G., Cardinal D., André L., Delstanche S. and Delvaux B. (2009) Impact of soil weathering degree on silicon isotopic fractionation during adsorption onto iron oxides in basaltic ash soils, Cameroon. *Geochim. Cosmochim. Acta* **73,** 7226-7240.

Opfergelt S., Cardinal D., André L., Delvigne C., Bremond L. and Delvaux B. (2010) Variations of δ^{30}Si and Ge/Si with weathering and biogenic input in tropical basaltic ash soils under monoculture. *Geochim. Cosmochim. Acta* **74,** 225-240.

Opfergelt S., Georg R. B., Burton K. W., Guicharnaud R., Siebert C., Gislason S. R. and Halliday A. N. (2011) Silicon isotopes in allophane as a proxy for mineral formation in volcanic soils. *Appl. Geochem.* **26,** S115-S118.

Opfergelt S., Georg R.B., Delvaux B., Cabidoche Y.-M., Burton K.W. and Halliday A.N. (2012) Silicon isotopes and the tracing of desilication in volcanic soil weathering sequences, Guadeloupe Chem. Geol. **326-327**, 113-122.

Pye K. (1995) The nature, origin and accumulation of loess. *Quat. Sci. Rev.* **14,** 653-667.

Ragueneau O., Tréguer P., Leynaert A., Anderson R. F., Brzezinski M. A., DeMaster D. J., Dugdale R. C., Dymond J., Fischer G., François R., Heinze C., Maier-Reimer E., Martin-Jézéquel V., Nelson D. M. and Quéguiner B. (2000) A review of the Si cycle in the modern ocean: Recent progress and missing gaps in the application of biogenic opal as a paleoproductivity proxy. *Global Planet. Change* **26,** 317-365.

Reynolds B. C., Aggarwal J., André L., Baxter D., Beucher C., Brzezinski M. A., Engström E., Georg R. B., Land M., Leng M. J., Opfergelt S., Rodushkin I., Sloane H. J., Van Den Boorn S. H. J. M., Vroon P. Z. and Cardinal D. (2007) An inter-laboratory comparison of Si isotope reference materials. *J. Anal. Atom. Spec.* **22,** 561-568.

Rudnick R. L. and Gao S. (2003) Composition of the continental crust, 1-64. In *The Crust* (ed. R.L. Rudnick) Vol 3 *Treatise on Geochemistry* (eds. H.D. Holland and K.K. Turekian). Elsevier-

Pergamon, Oxford.

Savage P. S., Georg R. B., Armytage R. M. G., Williams H. M. and Halliday A. N. (2010) Silicon isotope homogeneity in the mantle. *Earth Planet. Sci. Lett.* **295,** 139-146.

Savage P. S., Georg R. B., Williams H. M., Burton K. W. and Halliday A. N. (2011a) Silicon isotope fractionation during magmatic differentiation. *Geochim. Cosmochim. Acta* **75,** 6124-6139.

Savage P. S., Georg R. B., Williams H. M., Turner S., Halliday A. N. and Chappell B.W. (2012) The silicon isotope composition of granites. *Geochim. Cosmochim. Acta* **92,** 184-202.

Steinhoefel G., Breuer J., von Blanckenburg F., Horn I., Kaczorek D. and Sommer M. (2011) Micrometer silicon isotope diagnostics of soils by UV femtosecond laser ablation. *Chem. Geol.* **286,** 280-289.

Taylor S. R. and McLennan S. M. (1985) *The Continental Crust: Its Composition and Evolution.* Blackwell Scientific Publications.

Taylor S. R., McLennan S. M. and McCulloch M. T. (1983) Geochemistry of loess, continental crustal composition and crustal model ages. *Geochim. Cosmochim. Acta* **47,** 1897-1905.

Teng F. Z., McDonough W. F., Rudnick R. L., Dalpé C., Tomascak P. B., Chappell B. W. and Gao S. (2004) Lithium isotopic composition and concentration of the upper continental crust. *Geochim. Cosmochim. Acta* **68,** 4167-4178.

Tréguer P., Nelson D. M., Van Bennekom A. J., DeMaster D. J., Leynaert A. and Quéguiner B. (1995) The silica balance in the world ocean: A reestimate. *Science* **268,** 375-379.

Turner D. R., Dickson A. G. and Whitfield M. (1980) Water-rock partition coefficients and the composition of natural waters – a reassessment. *Mar. Chem.* **9,** 211-218.

Van Den Boorn S. H. J. M., Vroon P. Z. and Van Bergen M. J. (2009) Sulfur-induced offsets in MC-ICP-MS silicon-isotope measurements. *J. Anal. At. Spectrom.* **24**, 1111–1114.

Walker J. C. G., Hays P. B. and Kasting J. F. (1981) A negative feedback mechanism for the long-term stabilization of Earth's surface temperature. *J. Geophys. Res.* **86,** 9776-9782.

Wedepohl K.H. (1995) The composition of the continental crust. *Geochim. Cosmochim. Acta* **59,** 1217-

1232.

Weyer, S. and Schwieters, J. (2003) High precision Fe isotope measurements with high mass resolution MC-ICPMS. *Int. J. Mass Spectrom.* **226**, 355-368.

Wille M., Sutton J., Ellwood M.J., Sambridge M., Maher W., Eggins S. and Kelly M. (2010) Silicon isotopic fractionation in marine sponges: A new model for understanding silicon isotopic variations in sponges. *Earth Planet. Sci. Lett.*, **292 (3-4)**, 281-289

Zambardi T. and Poitrasson F. (2011) Precise Determination of Silicon Isotopes in Silicate Rock Reference Materials by MC-ICP-MS. *Geostand. Geoanal. Res.* **35,** 89-99.

Ziegler K., Chadwick O. A., Brzezinski M. A. and Kelly E. F. (2005a) Natural variations of δ^{30}Si ratios during progressive basalt weathering, Hawaiian Islands. *Geochimica et Cosmochimica Acta* **69,** 4597-4610.

Ziegler K., Chadwick O. A., White A. F. and Brzezinski M. A. (2005b) δ^{30}Si systematics in a granitic saprolite, Puerto Rico. *Geology* **33,** 817-820.

FIGURE CAPTIONS

Figure 1: Plot of $\delta^{30}Si$ values for the loess and shale samples analysed in this study (error bars are 95% s.e.), showing that loess is relatively homogeneous, and that shales define a large range of Si isotopic compositions. Also shown are $\delta^{30}Si$ values for I-, A- and S-type granites (Savage et al., 2012), extrusive igneous rocks (Savage et al., 2011) and Bulk Silicate Earth (Savage et al., 2010) for comparison.

Figure 2: Graph of $\delta^{30}Si$ against SiO_2 for all loess and shale samples (error bars are 95% s.e.) - see text for discussion. BSE value ($\delta^{30}Si$ = -0.29 ‰) is taken from Savage et al (2010); granite average ($\delta^{30}Si$ = -0.23 ‰; grey box ± 0.15 ‰ 2 s.d.) is taken from Savage et al. (2012).

Figure 3: Graph of $\delta^{30}Si$ against CIA value for a) all shale samples and b) all loess samples (error bars are 95% s.e.). The CIA value is defined as CIA = molar Al_2O_3/ [Al_2O_3+ CaO* + Na_2O+ K_2O], where CaO* refers to the CaO present only in silicates (Nesbitt and Young, 1982, McLennan, 1993). BSE value ($\delta^{30}Si$ = -0.29 ‰) is taken from Savage et al (2010); granite average ($\delta^{30}Si$ = -0.23 ‰; dark grey box ± 0.15 ‰ 2 s.d.) is taken from Savage et al. (2012).The light grey bar illustrates the range of CIA values for unweathered igneous material (50 ± 5; Nesbitt and Young, 1982). For the shale samples, a very vague negative trend exists between $\delta^{30}Si$ and CIA value (R^2 = 0.14), indicating a component of chemical weathering in the Si isotopic compositions of shales. No such relationship exists for loess. The Canadian samples have been plotted in both figures because the sample group contains both loess-like and shale-like samples.

Figure 4: Graph of $\delta^{30}Si$ against a) $\delta^{7}Li$ and b) $\delta^{26}Mg$ for the loess and shale samples, where available (error bars are 95% s.e.), which illustrates the large range of $\delta^{26}Mg$ and $\delta^{7}Li$ and small range of $\delta^{30}Si$ for the loess. Even though all three isotope systems are affected by weathering processes, there are no

771 strong relationships shown by the data.

772

773 **Figure 5:** Graph of $\delta^{30}Si$ against a) Al/Si ratio and b) Nb contents for loess and shales (symbols as in
774 Figure 3, error bars are 95% s.e.), which illustrates the good negative relationship between the two
775 (regression statistics calculated in Gnumeric; http://projects.gnome.org/gnumeric/). The average Al/Si
776 and Nb UCC compositions are taken from Rudnick and Gao (2003) and Barth et al., (2000); these
777 values correspond well to the average Si isotope loess composition. Similarly strong relationships exist
778 between $\delta^{30}Si$ and other insoluble elements; see text for discussion.

779

780 **Figure 6:** Modelled $\delta^{30}Si$ and Al/Si evolution of a putative "granite" starting composition (hereafter
781 "SC", star symbol) along various weathering and mixing trajectories (tick marks along each line are
782 10%). Shale and loess data are also plotted for comparison. The SC is composed of 40% quartz and
783 60% feldspar, with $\delta^{30}Si$ = -0.25 ‰ and Al/Si = 0.25. Scenarios A, B and C show various phase
784 transformations in the starting material: A) loss of feldspar/accumulation of quartz; B) replacement of
785 feldspar by smectite ($\delta^{30}Si$ = -1.1 ‰; Al/Si = 0.67) and loss of 25% of detrital quartz; C) replacement
786 of feldspar by kaolinite ($\delta^{30}Si$ = -2.0 ‰; Al/Si = 1.0) and loss of 60% of detrital quartz. Much of the
787 shale data lie on or close to lines B and C, suggesting secondary mineral formation and abundance of
788 detrital quartz are major controls over shale Si isotope composition. Scenario D shows simple mixing
789 between the SC and a biogenic silica source ($\delta^{30}Si$ = +1.24 ‰; Al/Si = 0) and implies that only ~10%
790 incorporation of such material is needed to explain the heavier isotopic compositions of some of the
791 shales. See text for discussion.

792

793 **Figure 7:** Histogram of the $\delta^{30}Si$ values of the upper crustal lithologies analysed in this study and the
794 granite study of Savage et al. (2012). One clear peak, around $\delta^{30}Si$ = -0.25 to -0.20 ‰, is defined
795 mainly by the granites and loess samples. This peak also coincides with the weighted average $\delta^{30}Si$

796 value for the upper continental crust. BSE average is taken from Savage et al. (2010).

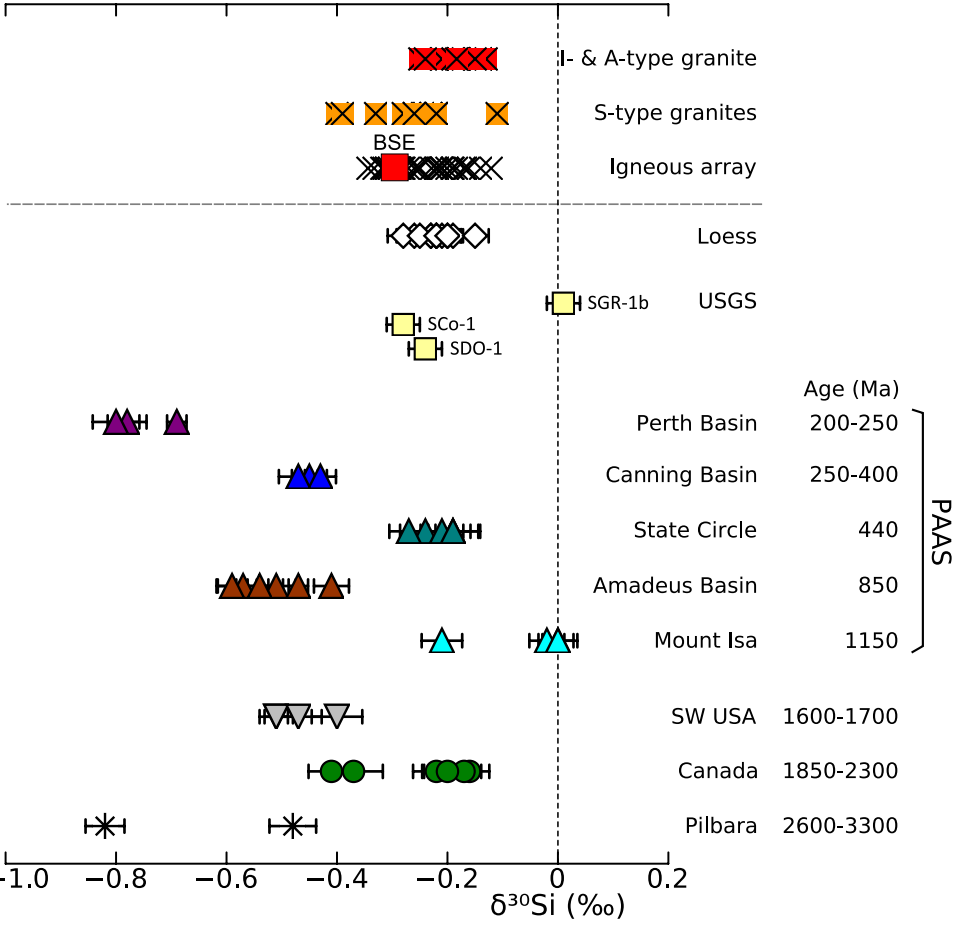
I- & A-type granite
S-type granites
BSE
Igneous array
Loess
USGS
SGR-1b
SCo-1
SDO-1
Age (Ma)
Perth Basin
200-250
Canning Basin
250-400
State Circle
440
Amadeus Basin
850
Mount Isa
1150
PAAS
SW USA
1600-1700
Canada
1850-2300
Pilbara
2600-3300
−1.0
−0.8
−0.6
−0.4
−0.2
0
0.2
δ30Si (‰)

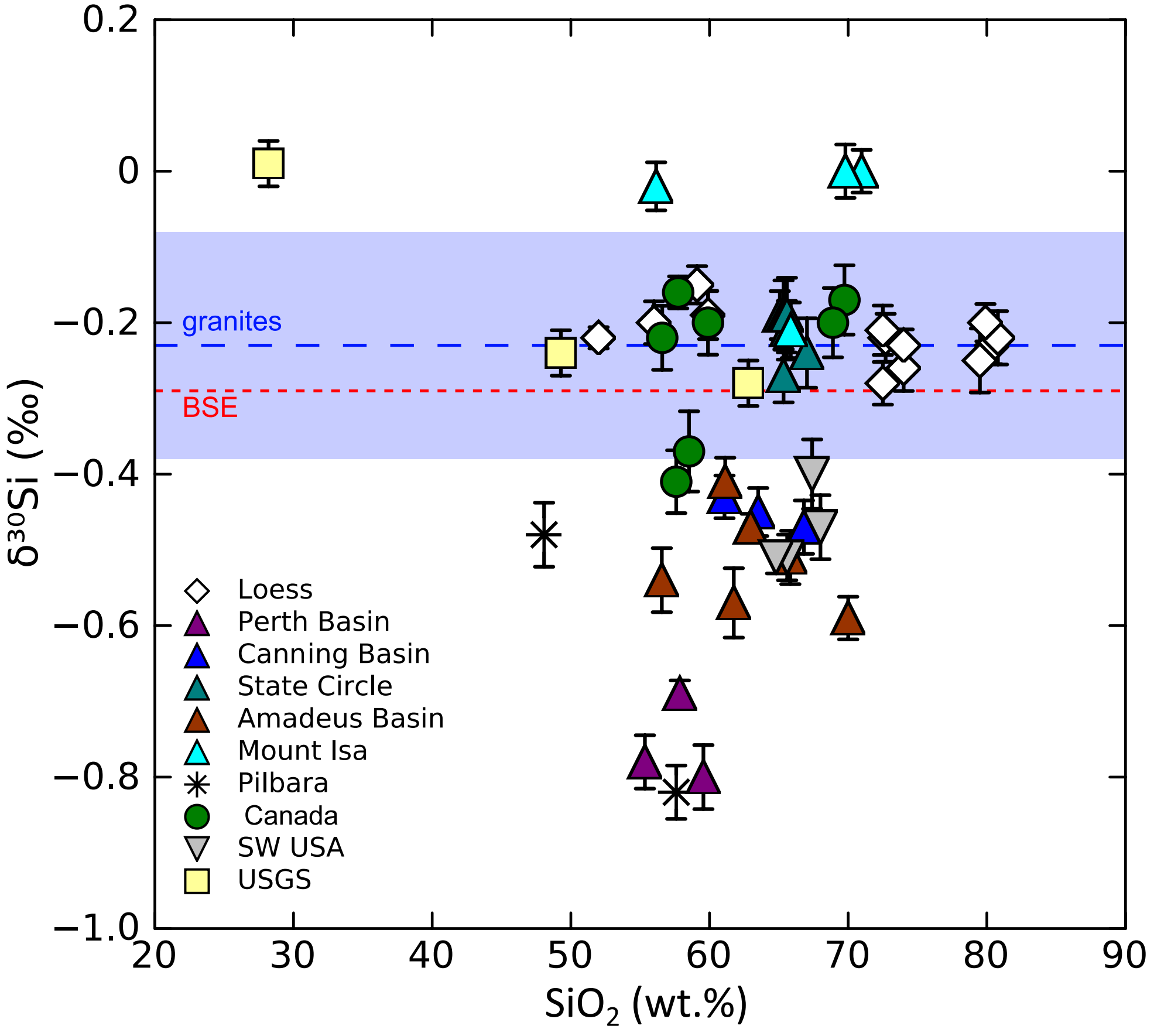
0.2
0
−0.2
−0.4
−0.6
−0.8
−1.0
20
30
40
50
60
70
80
90
δ30Si (‰)
SiO2 (wt.%)
granites
BSE
Loess
Perth Basin
Canning Basin
State Circle
Amadeus Basin
Mount Isa
Pilbara
Canada
SW USA
USGS

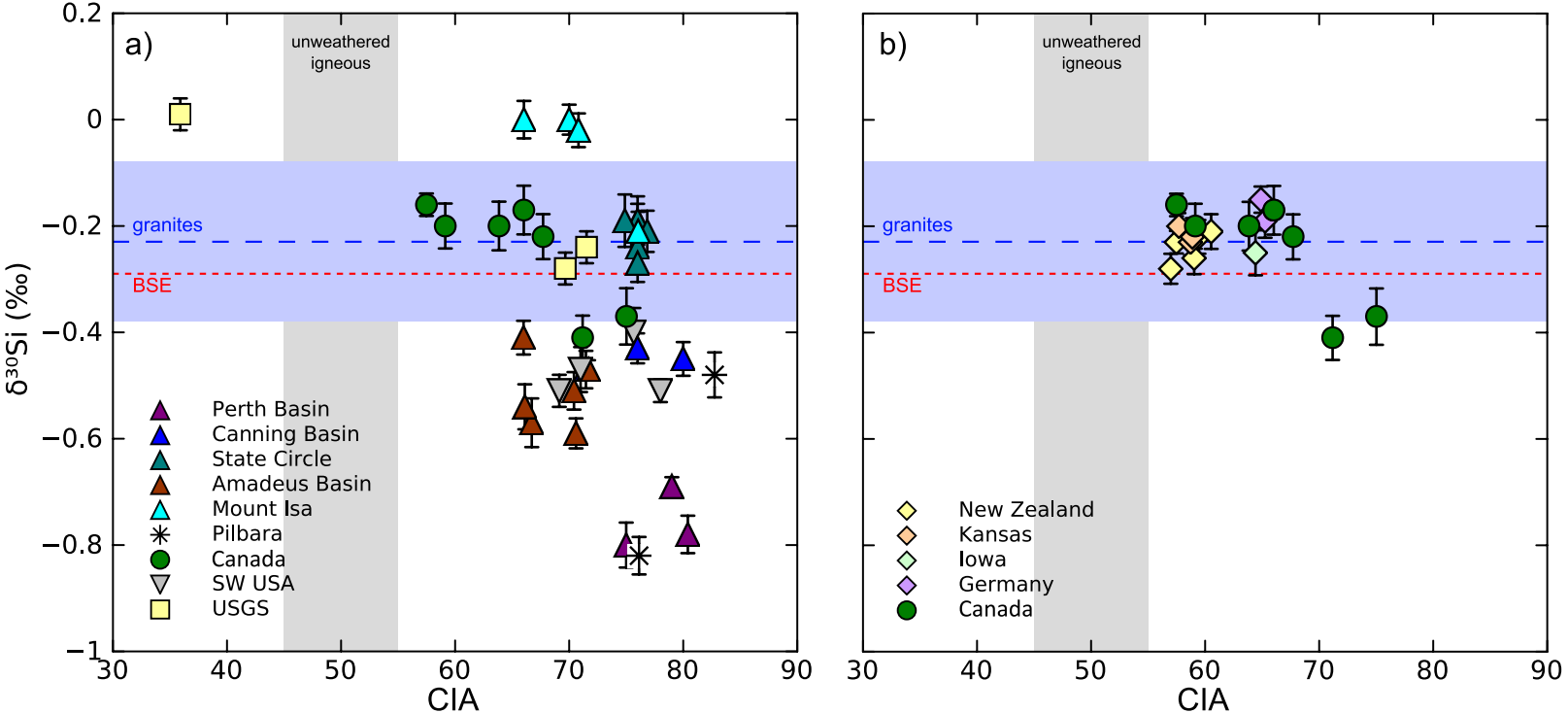
a)
b)
unweathered igneous
granites
BSE
δ30Si (‰)
CIA
Perth Basin
Canning Basin
State Circle
Amadeus Basin
Mount Isa
Pilbara
Canada
SW USA
USGS
New Zealand
Kansas
Iowa
Germany
Canada

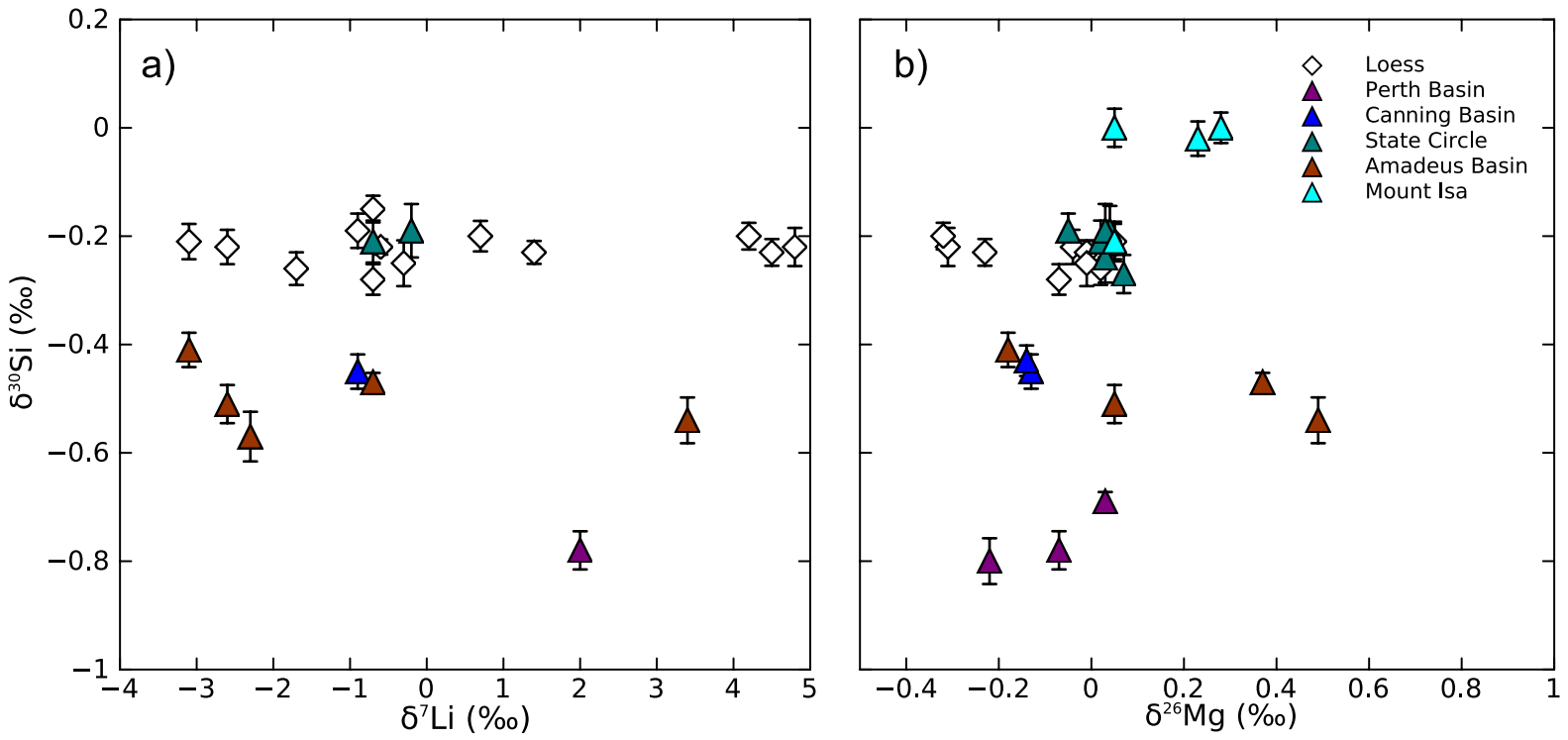
a)
b)
Loess
Perth Basin
Canning Basin
State Circle
Amadeus Basin
Mount Isa
δ30Si (‰)
δ7Li (‰)
δ26Mg (‰)
0.2
0
−0.2
−0.4
−0.6
−0.8
−1
−4
−3
−2
−1
0
1
2
3
4
5
−0.4
−0.2
0
0.2
0.4
0.6
0.8
1

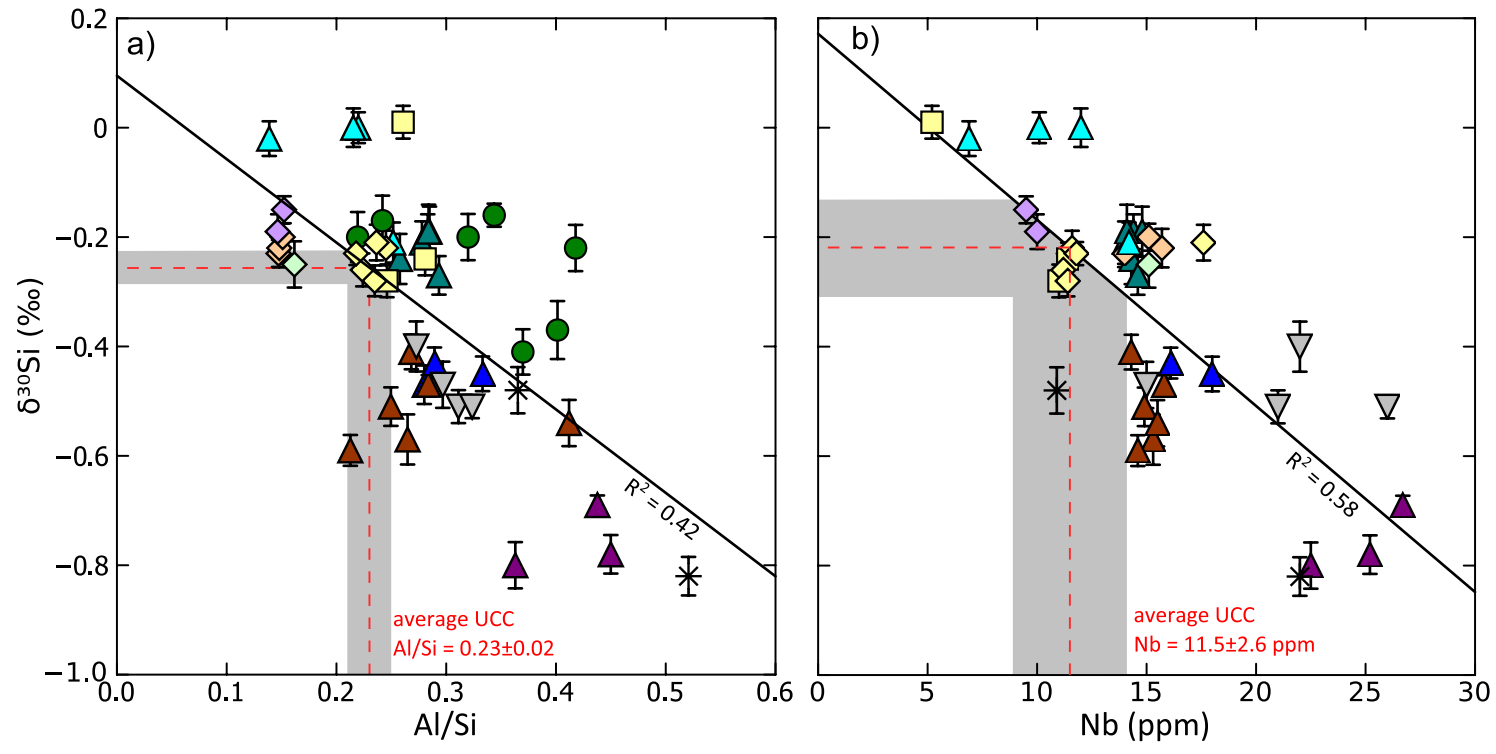
a)
b)
δ30Si (‰)
Al/Si
Nb (ppm)
R2 = 0.42
R2 = 0.58
average UCC
Al/Si = 0.23±0.02
average UCC
Nb = 11.5±2.6 ppm

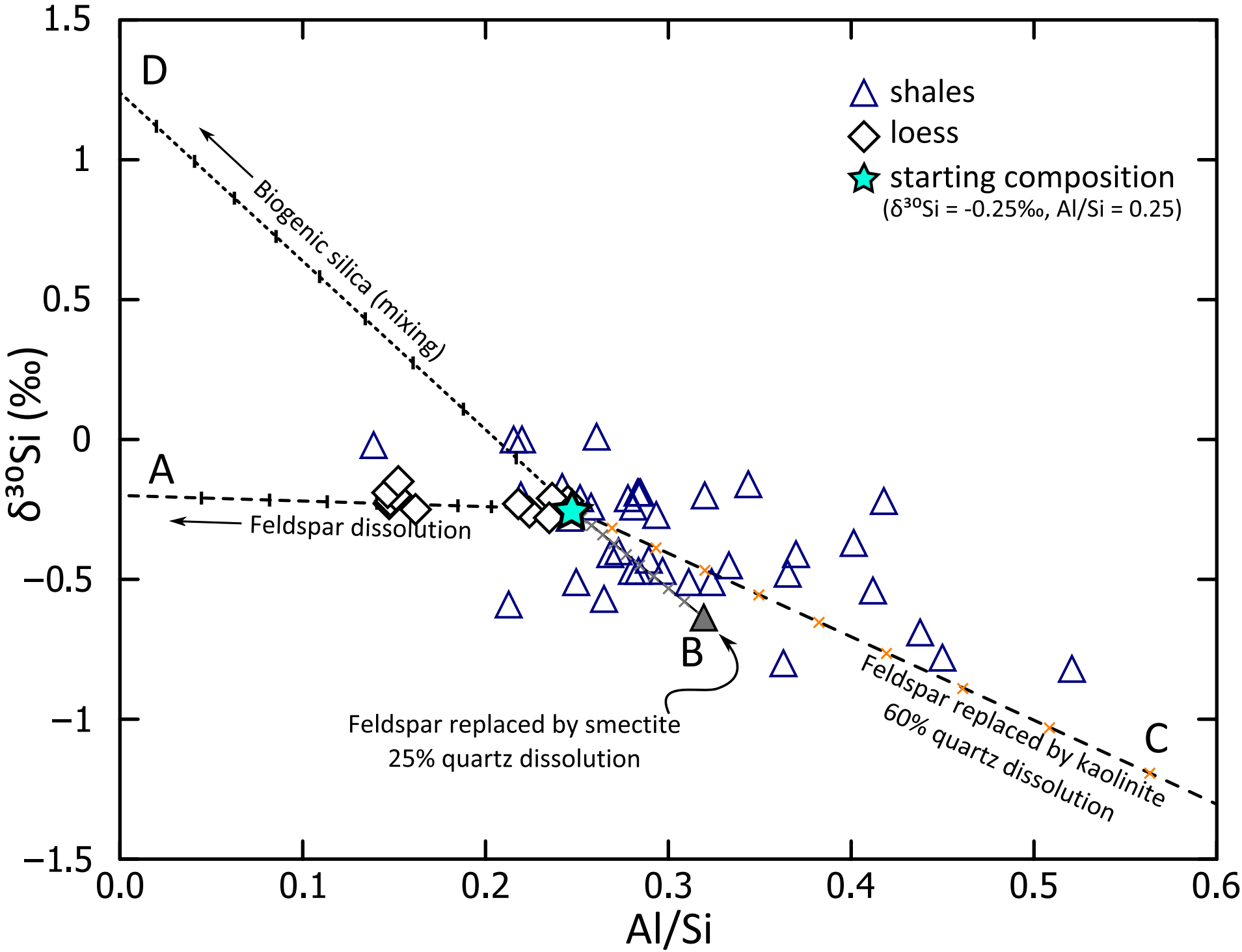
shales
loess
starting composition
(δ30Si = -0.25‰, Al/Si = 0.25)
D
A
B
C
Biogenic silica (mixing)
Feldspar dissolution
Feldspar replaced by smectite
25% quartz dissolution
Feldspar replaced by kaolinite
60% quartz dissolution
δ30Si (‰)
Al/Si
1.5
1
0.5
0
−0.5
−1
−1.5
0.0
0.1
0.2
0.3
0.4
0.5
0.6

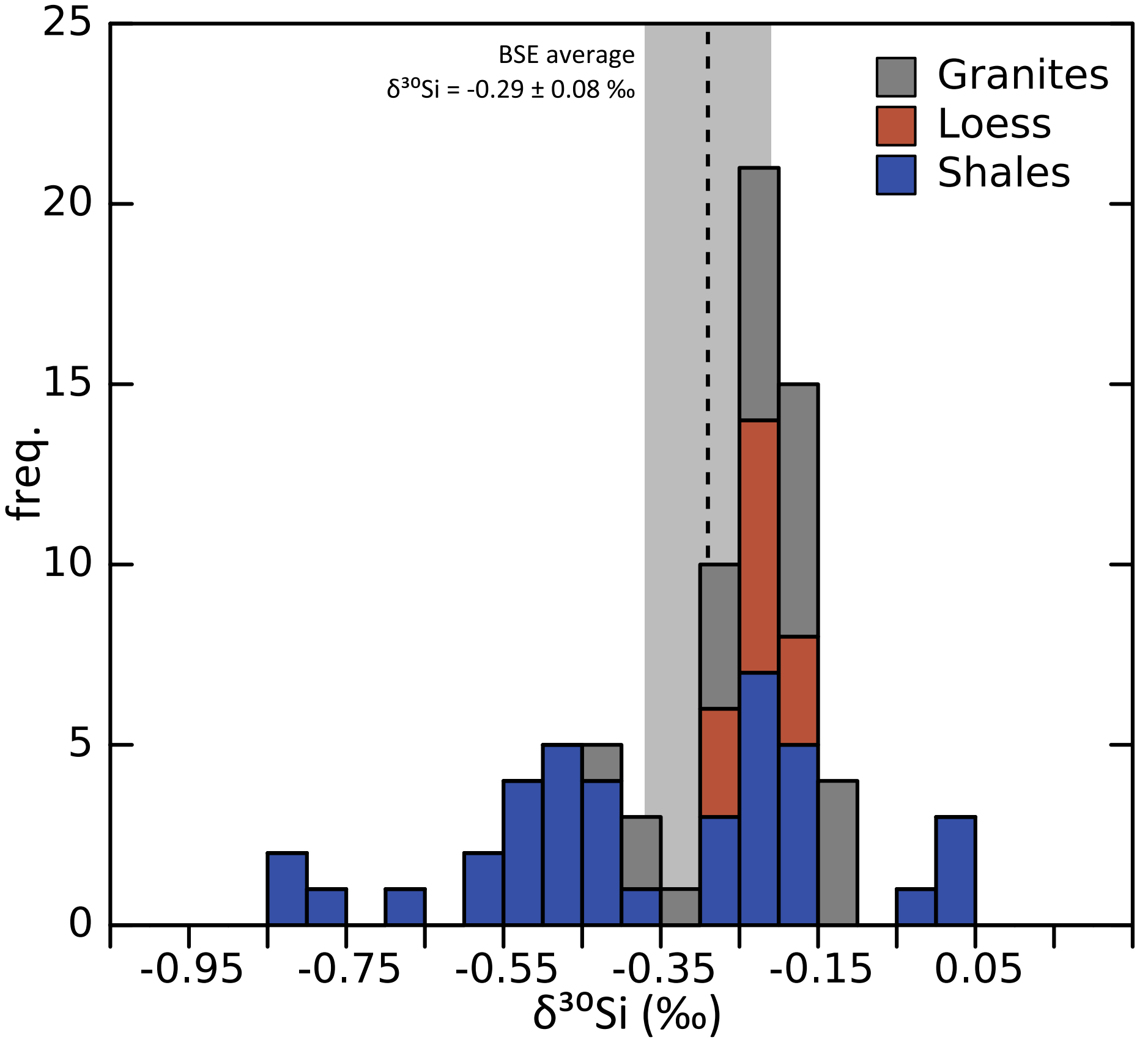
BSE average
δ³⁰Si = -0.29 ± 0.08 ‰
Granites
Loess
Shales
freq.
25
20
15
10
5
0
-0.95
-0.75
-0.55
-0.35
-0.15
0.05
δ³⁰Si (‰)

Table 1.

Silicon isotope data for external standards analysed during this study, as well as literature values for said standards. Numbers refer to repeat analysis of the same solution. Errors are given as both 2 s.d. (2 × standard deviation) and 95% s.e. (95% standard error of the mean = t × s.d./$(n)^{1/2}$, where t = inverse survival function of the Student's t-test at the 95% significance level, and n-1 degrees of freedom).

Standard		**SiO_2 (wt.%)**	**$\delta^{30}Si$ (‰)**	**2s.d.**	**95%s.e.**	**$\delta^{29}Si$ (‰)**	**2s.d.**	**95%s.e.**	***n***
Diatomite	1	100	1.22	0.11	0.04	0.64	0.07	0.02	11
	2		1.23	0.09	0.03	0.62	0.06	0.02	11
	3		1.22	0.07	0.02	0.64	0.07	0.02	11
	4		1.21	0.04	0.02	0.59	0.05	0.02	11
	5		1.20	0.08	0.03	0.61	0.07	0.02	11
	6		1.25	0.08	0.03	0.63	0.07	0.02	11
	7		1.23	0.10	0.04	0.63	0.07	0.02	11
	8		1.20	0.06	0.02	0.63	0.03	0.01	11
	9		1.22	0.09	0.03	0.62	0.08	0.03	11
	10		1.24	0.11	0.04	0.61	0.07	0.02	10
	11		1.23	0.10	0.03	0.65	0.11	0.04	11
	12		1.20	0.10	0.04	0.61	0.05	0.02	9
Mean and external reproducibility			1.22	0.03		0.62	0.03		12
Reynolds et al. (2007)			1.26	0.20		0.64	0.14		
Georg et al. (2009a)			1.23	0.16		0.62	0.11		
Savage et al. (2011)			1.23	0.10		0.64	0.08		
SGR-1b	1	28.2	0.01	0.04	0.01	-0.01	0.06	0.02	11
Hughes et al. (2011)			0.03	0.09		0.02	0.03		
BHVO-2	1	49.9	−0.31	0.05	0.02	−0.14	0.08	0.03	11
	2		−0.34	0.10	0.03	−0.15	0.06	0.02	11
	3		−0.29	0.06	0.02	−0.18	0.04	0.01	11
	4		−0.26	0.05	0.02	−0.13	0.07	0.02	11
	5		−0.29	0.07	0.02	−0.17	0.06	0.02	11
	6		−0.31	0.08	0.03	−0.14	0.03	0.01	11
	7		−0.31	0.10	0.03	−0.15	0.09	0.03	11
	8		−0.29	0.12	0.04	−0.16	0.07	0.02	11
	9		−0.31	0.08	0.03	−0.17	0.08	0.03	10
	10		−0.33	0.10	0.04	−0.16	0.09	0.03	9
	11		−0.28	0.06	0.02	−0.15	0.04	0.01	11

12	−0.30	0.10	0.03	−0.17	0.06	0.02	11
Mean and external reproducibility	−0.30	0.04		−0.16	0.03		12
Abraham et al. (2008)	−0.29	0.11		−0.17	0.04		
Zambardi and Poitrasson (2011)	−0.27	0.08		−0.14	0.05		
Savage et al. (2011)	−0.29	0.09		−0.15	0.08		

Table 2.

Silicon isotope data for loess samples analysed in this study. Major element data and CIA values are taken from Taylor et al. (1983). Magnesium and lithium stable isotope data are taken from Li et al. (2010) and Teng et al. (2004) respectively.

Sample	ID	SiO_2 (wt. %)	$\delta^{30}Si$ (‰)	2s.d.	95%s.e.	$\delta^{29}Si$ (‰)	2s.d.	95%s.e.	*n*	CIA	$\delta^{26}Mg$ (‰)	$\delta^{7}Li$ (‰)	Al/Si
Banks Peninsula, New Zealand	BP-1	72.7	-0.22	0.09	0.03	-0.12	0.06	0.02	11	59	-0.04	-2.6	0.25
	BP-2	74.0	-0.26	0.08	0.03	-0.12	0.04	0.02	10	59	0.02	-1.7	0.22
	BP-3	72.5	-0.21	0.08	0.03	-0.08	0.06	0.02	9	61	0.05	-3.1	0.24
	BP-4	74.0	-0.23	0.06	0.02	-0.12	0.07	0.02	11	57	-0.01	1.4	0.22
	BP-5	72.5	-0.28	0.08	0.03	-0.11	0.05	0.02	11	57	-0.07	-0.7	0.23
Kansas, USA	CY-4a-A	80.4	-0.23	0.07	0.02	-0.12	0.11	0.04	11	59	-0.23	4.5	0.15
	CY-4a-B	80.8	-0.22	0.10	0.04	-0.12	0.07	0.02	11	59	-0.31	4.8	0.15
	CY-4a-C	79.9	-0.20	0.07	0.02	-0.10	0.04	0.01	11	58	-0.32	4.2	0.15
Muscatine, Iowa, USA	I	79.5	-0.25	0.12	0.04	-0.13	0.02	0.02	11	64	-0.01	-0.3	0.16
Kaiserstuhl, Germany	K1	59.9	-0.19	0.09	0.03	-0.09	0.06	0.02	11	65		-0.9	0.15
	K2	59.1	-0.15	0.07	0.02	-0.08	0.06	0.02	11	65		-0.7	0.15
Hungary	H	52.0	-0.22	0.04	0.01	-0.14	0.04	0.01	11			-0.6	
China	CH	56.0	-0.19	0.11	0.04	-0.11	0.07	0.03	10			0.7	
	CH-repeat		-0.20	0.08	0.03	-0.08	0.08	0.03	11				

Table 3.

Silicon isotope data for shale samples analysed in this study. Silica contents (in wt. %) and deposition ages are taken from Taylor and McLennan (1976), McLennan et al., (1995) and the UGSG datasheets (http://minerals.cr.usgs.gov/). CIA values are taken directly from, or calculated using the chemical analyses provided in the above papers. Magnesium and lithium stable isotope data are taken from Li et al. (2010) and Teng et al. (2004) respectively.

Sample	ID	SiO_2 (wt.%)	$\delta^{30}Si$ (‰)	2s.d.	95%s.e.	$\delta^{29}Si$ (‰)	2s.d.	95%s.e.	*n*	CIA	$\delta^{26}Mg$ (‰)	$\delta^{7}Li$ (‰)	Al/Si
Post-Archaean Australian shales													
Perth Basin	PW-4	57.9	-0.69	0.05	0.02	-0.37	0.11	0.04	11	79	0.02		0.44
(200-250 Ma)	PW-5	55.3	-0.78	0.10	0.04	-0.41	0.08	0.03	11	80	-0.07	2.0	0.45
	PW-7	59.6	-0.80	0.12	0.04	-0.41	0.13	0.05	11	75	-0.22		0.36
Canning Basin	PL-1	63.5	-0.45	0.09	0.03	-0.21	0.07	0.02	11	80	-0.13	-0.9	0.33
(250-400 Ma)	PL-6	61.1	-0.43	0.08	0.03	-0.25	0.03	0.01	11	76	-0.14		0.29
	PL-7	66.8	-0.47	0.10	0.04	-0.22	0.05	0.02	11	71			0.28
State Circle	SC-1	65.1	-0.19	0.09	0.03	-0.09	0.08	0.03	11	76	-0.05		0.28
(440 Ma)	SC-2	65.3	-0.19	0.13	0.05	-0.08	0.10	0.04	11	76	0.04		0.28
	SC-3	67.0	-0.24	0.13	0.05	-0.15	0.07	0.02	11	76	0.03		0.26
	SC-5	65.3	-0.27	0.10	0.04	-0.14	0.12	0.04	11	76	0.07		0.29
	SC-7	65.6	-0.21	0.11	0.04	-0.14	0.04	0.01	11	77	0.02	-0.7	0.28
	SC-8	65.6	-0.19	0.14	0.05	-0.11	0.08	0.03	11	75	0.03	-0.2	0.28
Amadeus Basin	AO-6	61.1	-0.41	0.09	0.03	-0.22	0.07	0.02	11	66	-0.18	-3.1	0.27
(850 Ma)	AO-7	61.8	-0.57	0.13	0.05	-0.28	0.10	0.04	11	67		-2.3	0.26

	AO-8	70.0	-0.59	0.08	0.03	-0.31	0.08	0.03	11	71			0.21
	AO-9	65.8	-0.51	0.10	0.04	-0.29	0.08	0.03	11	70	0.05	-2.6	0.25
	AO-10	63.0	-0.47	0.05	0.02	-0.27	0.03	0.01	11	72	0.37	-0.7	0.28
	AO-12	56.6	-0.54	0.12	0.04	-0.28	0.05	0.02	11	66	0.49	3.4	0.41
Mt. Isa	MI-1	71.0	0.00	0.08	0.03	-0.01	0.07	0.02	11	70	0.28		0.22
(1500 Ma)	MI-2	56.1	-0.02	0.09	0.03	-0.01	0.06	0.02	11	71	0.23		0.14
	MI-4	69.8	0.00	0.10	0.04	-0.02	0.07	0.02	11	66	0.05		0.22
	MI-5	65.9	-0.21	0.09	0.04	-0.14	0.09	0.04	9	76	0.05		0.25
Pilbara Archaean shales - Australia													
Gorge Creek (3.4 Ga)	Pg-7	57.6	-0.82	0.10	0.04	-0.41	0.08	0.03	11	76			0.52
Whim Creek (2.7 Ga)	WC-3	48.1	-0.48	0.12	0.04	-0.21	0.09	0.03	11	82			0.37
Huronian – Canada (2.5 – 2.2 Ga)													
McKim	M-5	58.5	-0.37	0.13	0.05	-0.21	0.05	0.02	9	75			0.40
Pecors	P-7	56.6	-0.22	0.12	0.04	-0.09	0.11	0.04	11	68			0.42
Gowganga	G-9	59.9	-0.20	0.12	0.04	-0.09	0.04	0.01	11	59			0.32
	G-9repeat		-0.18	0.09	0.03	-0.07	0.04	0.02	10				
	G-16	57.7	-0.16	0.06	0.02	-0.07	0.05	0.02	11	57			0.34
	G-28	57.6	-0.41	0.11	0.04	-0.21	0.11	0.04	10	71			0.37
Gordon Lake	GL-3		-0.17	0.13	0.05	-0.10	0.07	0.02	11	66			0.24
Sudbury Basin – Canada (1.85 Ga)													
Chelmsford	DKM-6	68.9	-0.20	0.13	0.05	-0.10	0.06	0.02	11	64			0.22
SW USA Protorezoic (1.8 -1.7 Ga)													
Rinconada	R1-1	65.6	-0.51	0.08	0.03	-0.30	0.05	0.02	10	69			0.31
	R4-5	64.8	-0.51	0.06	0.02	-0.27	0.10	0.04	11	78			0.32

Piedra Lumbra	PL-5	68.0	-0.47	0.12	0.04	-0.26	0.13	0.05	11	71	0.30
Uncomphagre	S-4	67.4	-0.40	0.13	0.05	-0.22	0.08	0.03	11	76	0.27
USGS shale standards											
Ohio - Devonian	SDO-1	49.3	-0.24	0.04	0.01	-0.10	0.07	0.02	11	72	0.28
Cody - Cretaceous	SCo-1	62.8	-0.28	0.03	0.01	-0.17	0.04	0.01	11	70	0.25
Gren River - Eocene	SGR-1b	28.2	0.01	0.04	0.01	-0.01	0.06	0.02	11	36	0.26

Table 4.

Estimate of the weighted average Si isotopic composition of the upper continental crust, as well as calculated $\delta^{30}Si$ averages for the component lithologies. Lithological units, proportions and SiO_2 contents are taken from Wedepohl (1995), except for the sedimentary sub-unit SiO_2 contents, which were estimated using the samples analysed in this study. The sedimentary $\delta^{30}Si$ was calculated using data from this research; the felsic intrusive unit was constrained using data from Savage et al. (2012); the $\delta^{30}Si$ value of the gabbroic unit is the BSE value (Savage et al., 2010).

Rock Unit	**Proportion in upper crust (%)**	**Avg. SiO_2 (wt.%)**	**$\delta^{30}Si$ (‰)**	**2s.d.**
Sedimentary	14	52.4	-0.31	0.26
Sub-units	of which			
Shales, siltstones	6	61.7	-0.36	0.44
Sandstones	3	73.2	-0.22	0.07
Mafic volcanics	3	50.1	-0.29	0.08
Carbonates	2	0	-	-
Felsic intrusive	50	69.2	-0.23	0.15
Gabbro	6	50.1	-0.29	0.08
Metamorphic	30	63.7	-0.25	0.16
Upper continental crust		64.1	-0.25	0.16